The Effects of Uniform Acceleration on the Correlation Harvesting

by

Manar Naeem

A thesis
presented to the University of Waterloo
in fulfillment of the
thesis requirement for the degree of
Master of Science
in
Physics (Quantum Information)

Waterloo, Ontario, Canada, 2023

Author's Declaration

This thesis consists of material all of which I authored or co-authored: see Statement of Contributions included in the thesis. This is a true copy of the thesis, including any required final revisions, as accepted by my examiners.

I understand that my thesis may be made electronically available to the public.

Statement of Contributions

The thesis is based on the following published and forthcoming articles.

- Chapter 3 is based on

  Manar Naeem, Kensuke Gallock-Yoshimura, and Robert B. Mann, Mutual information harvested by uniformly accelerated particle detectors, Phys. Rev. D 107, 065016 (2023)

- Chapter 4 is based on

  Lana Bozanic, **Manar Naeem**, Kensuke Gallock Yoshimura, and Robert B. Mann, Correlation harvesting between particle detectors in uniform motion, arXiv:2308.06329 [quant-ph] (2023)

Abstract

Quantum field theory (QFT) in curved spacetime focuses on the analysis of quantum fields—representing fundamental particles and their interactions—within a curved spacetime geometry, accounting for relativistic effects.

Among the prominent subjects in QFT are the Unruh effect and the entanglement harvesting protocol. The Unruh effect, introduced by G. Unruh [1], posits that a uniformly accelerating particle detector undergoes thermality, despite the absence of particles perceived by an inertial observer. Entanglement harvesting protocol on the other hand involves two or more Unruh-Dewitt (UDW) detectors within a quantum field. It examines the amount of entanglement between these detectors after interacting with the field, which depends on the trajectories of the detectors and the spacetime geometry. Current studies are expanding into other correlation types, collectively referred to as the correlation harvesting protocol.

In this thesis, we investigate the effects of uniform acceleration on the correlation harvesting protocol, with a particular emphasis on understanding the impact of Unruh temperature on the total correlation harvesting. A prior investigation [2] explored the correlation harvesting protocol for two inertial UDW detectors in a thermal bath. The findings revealed that high temperatures inhibit entanglement harvesting between the detectors, while it enhances the total correlation between them. We investigate whether the Unruh temperature induces a similar impact on correlation harvesting by examining the correlation harvesting protocol of two linearly uniformly accelerating UDW detectors. We then broaden our investigation to encompass other uniformly accelerating trajectories, initially defined by Letaw [3], that could induce effects similar to the Unruh effect, but might be more feasible than linear motion in an experimental setting, This is particularly relevant in consideration of ongoing experiments aiming for Unruh effect verification[4, 5, 6, 7, 8, 9]

Our findings are as follows: (i) high accelerations(equivalently Unruh temperature) prevent the detectors from acquiring correlations from the field in all trajectories of detectors that are uniformly accelerating. (ii) Within the framework of uniform acceleration, there exists small, yet consequential, regions of parameter space where detectors in causal contact may genuinely harvest entanglement. (iii) The Unruh temperature's effect on total correlation harvesting diverges from that of thermal bath temperature despite their similar effect on a single detector.

Acknowledgements

I would like to thank my supervisor, Dr. Robert Mann for being such a great example and a true inspiration for me. Thanks for being patient, and supportive you helped me love Physics more.

Thanks to my colleague and friend Kensuke Gallock-Yoshimura for your unlimited help and support throughout my degree, your passion for Physics is contagious.

I would like to thank my colleagues and collaborators Lana Bozanic, Maria Rosa Preciado Rivas, Massimiliano Spadafora, and Amit Anand. I learned alot from you.

Thanks to my parents Seham Badrieh and Mahmoud Naeem, you are the reason behind all my life accomplishments.

Thanks to my siblings, my source of support, and hope, Mohab, Maha, Fares, Feras, and Majd.

Thanks to my best friend Hiba ElMiari, the source of my happiness and inspiration. Your name says it all. You are one of the best gifts life has given me.

Thanks to my friends and second family, Mayar Nahed, Roula Karawi, Evaggelia Bisketzi, Lamees Audeh, Wafa Al Zagal, Nawrooz Kafaf, and Nour Khedder. Your presence in my life is priceless.

Thanks to my aunts Fawzia Badrieh, and Jadaa Badrieh. Your immense support is unforgettable.

Thanks to my Oud instrument and my cat Luna for the unlimited love and happiness you keep giving me.

Dedication

To my mother, Seham Badrieh: You are my inspiration and the reason behind all my successes in life. I wouldn't have gotten this far without you.

To my father, Mahmoud Naeem: You are my example of hard work and dedication.

To the soul of my uncle Fawaz Badrieh. Your memory will always be cherished...

Table of Contents

List of Figures

Chapter 1

Introduction

Quantum Field Theory (QFT) stands as a vital and rapidly advancing branch in theoretical physics. It provides the essential framework for the understanding of particle behavior at both quantum and relativistic levels and has spawned far-reaching implications across diverse domains such as particle physics, cosmology, and condensed matter physics[10, 11]. The ongoing exploration and growth of QFT is leading to new insights into multiple fields such as understanding the dynamics of black holes[12, 13] and facilitating more realistic developments in quantum information with including relativistic effects.

Relativistic quantum information (RQI), is the field that studies the effects of special and general relativity on quantum information processes. While quantum information deals with information processing using quantum systems, relativity describes the structure of space-time and the way objects move within it. By considering them together, RQI attempts to formulate a better understanding on fundamental questions about the nature of reality, information, and the structure of the universe. In relativistic quantum information, it is common to employ a localized qubit model known as Unruh-DeWitt (UDW) particle detector [1, 14], which interacts with quantum fields in spacetime. By using such a qubit model, one can examine, for example, the channel capacity of quantum fields [15, 16, 17, 18, 19] and the relativistic quantum teleportation protocol [20, 21].

One of the protocols that utilizes UDW model is the *entanglement harvesting protocol* which was first examined by Valentini in 1991[22] and subsequently Renzik et al. in the early 2000s[23, 24]. The protocol is the following: suppose two observers with a UDW detector are in a (flat or curved) spacetime on which a quantum field is defined. Assuming the detectors are initially uncorrelated, by locally interacting with the quantum field, the detectors become entangled after the interaction. This is true even when the observers are

causally disconnected because the quantum field is already in an entangled state [25, 26]. More generally, the detectors are extracting correlations from the quantum field, and so we can refer to the protocol as the *correlation harvesting protocol*. These correlations can be entanglement, mutual information, or quantum discord [27, 28, 29, 30]. The amount of correlation extracted is influenced by the geometry of spacetime [31, 32, 33, 34, 35, 36, 37] and the states of motion of the detectors [38, 39, 40].

Numerous studies have been conducted of the effects of temperature on correlation harvesting. The earliest investigation was carried out by Ver Steeg and Menicucci [41]. They found that, while a single detector in de Sitter spacetime responds as if it is in a thermal bath in Minkowski spacetime, the harvested entanglement between two detectors differs in de Sitter spacetime and a thermal bath. Since then, the temperature dependence of correlations in various scenarios has been analyzed. A basic scenario consists of two inertial detectors interacting with a field in a thermal state. In [42, 43] it was found that the amount of entanglement decreases with temperature whereas quantum mutual information increases monotonically. One can also think of two uniformly accelerating detectors in Minkowski spacetime. For a single particle detector, it is widely known that a detector undergoing uniform acceleration a experiences a thermal bath at temperature $T_{\mathrm{U}} = \hbar a/2\pi k_{\mathrm{B}} c$ which is called the Unruh effect [1] as mentioned earlier, and the temperature T_{U} is called the Unruh temperature. In this case, the field is in the Minkowski vacuum state instead of a thermal state, but due to its motion the detector responds in the same manner as if it were in the thermal quantum field. The harvested entanglement by uniformly accelerated detectors, however, shows a different temperature dependence in contrast to that of a thermal state; entanglement is enhanced at relatively smaller temperatures, then decreases and drops to 0 as the detectors experience hotter Unruh temperature [44].

One could ask if the behavior induced by acceleration is present in black hole spacetimes, since the Rindler metric is similar to the Schwarzschild one near its event horizon. Investigations of entanglement harvesting outside of black holes, while indicating there are indeed common features, have also found some surprising results, including the presence of an entanglement shadow near the horizon [34] and the amplification of harvested entanglement for near-extremal rotating black holes [45]. Other kinds of black hole spacetimes have been shown to exhibit other novel features [46, 47, 48, 45, 49, 50, 51]. In general, correlations steeply decline whereas excitation responses of detectors tend to increase as one of the static detectors is placed increasingly close to the horizon, where the black hole temperature is extremely high. The aforementioned studies (inertial detectors in a thermal quantum field, uniformly accelerated detectors in Minkowski vacuum, and static detectors in a black hole spacetime) have one thing in common: a single detector experiences a thermal bath at the corresponding temperature. That is, the response of the detector against

temperature is the same in all these cases. Yet the entanglement harvested between two detectors exhibits different temperature dependence, distinguishing the two scenarios from each other.

Quantum mutual information has been considerably less explored. The importance of studying quantum mutual information arises from its applications in multiple areas such as quantum communication [52] and quantum error correction [53]. A recent study [54] explicitly examined the relationship between quantum mutual information and the Bañados-Teitelboim-Zanelli (BTZ) black hole temperature. Unlike the case for entanglement harvesting, harvested mutual information vanished only when a (static) detector was placed arbitrarily close to the event horizon. It was the extremity of Hawking and Unruh effects near the horizon that inhibited the detectors from harvesting. In other words, the mutual information between two static detectors decreases, vanishing at high black hole temperatures.

In this thesis, we investigate the effects of uniform acceleration on the correlation harvesting protocol across various trajectories, endeavoring to identify more efficient trajectories suitable for experimental settings. A significant challenge hindering the experimental verification of the Unruh effect resides in the immense acceleration required to produce experimentally measurable temperatures. For instance, an acceleration on the order of magnitude of $a \approx 10^{20}\,\mathrm{m/s^2}$ is necessary to reach a temperature of $T_{\mathrm{U}} \sim 1$ Kelvin. Given this constraint, the focus is shifting towards the exploration of alternative detector trajectories that may induce phenomena akin to the Unruh effect. As a consequence, we are particularly interested in how the correlation harvesting protocol is influenced by the Unruh temperature and other types of acceleration-induced temperature.

In chapter 3 we try to complete the picture of the temperature dependence of correlation harvesting (we illustrate in Fig. 1.1 the qualitative distinctions between the various scenarios). Specifically we analyze the quantum mutual information harvested between two uniformly accelerating detectors where we consider three configurations of accelerating detector pairs – parallel, anti-parallel, and perpendicular [55] – and compare mutual information harvesting and entanglement harvesting with changing acceleration. We find that harvested quantum mutual information behaves in a broadly qualitatively similar way to harvested entanglement. For all three configurations of acceleration, both harvested mutual information and entanglement are enhanced at low temperatures, but become extinguished in the high Unruh temperature limit. We will comment on how to understand differences in the temperature dependence of correlation harvesting illustrated in Fig. 1.1 from the Wightman function perspective.

In Chapter 4 we investigate the correlation harvesting protocol with detectors in four

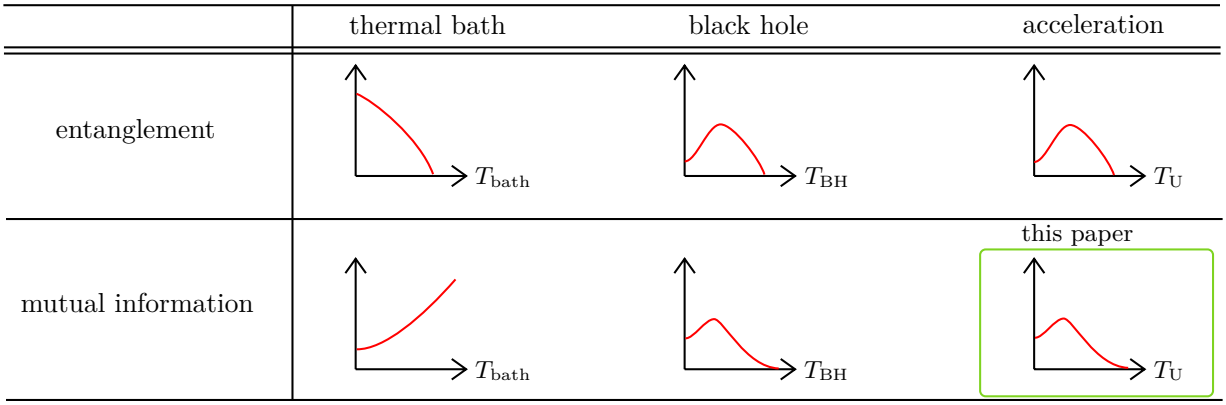

Figure 1.1: A summary of past results on the temperature dependence of correlation harvesting. Our results provide the case of mutual information with accelerating detectors as depicted in the lower-right corner.

classes of uniform acceleration motion categorized by Letaw [3]: linear, catenary, cusped, and circular trajectories. Unlike the helical case, these motions can all be realized in 2 spatial dimensions, and so are more amenable to experimental testing [4, 5, 6, 7, 8, 9]. In $(3+1)$-dimensional Minkowski spacetime, these trajectories are characterized by three parameters: two torsions and the magnitude of the proper acceleration. We classify the configurations for the detectors into two configurations: stationary, in which the Wightman function is time-translation invariant, and nonstationary, in which the Wightman function is not time-translation invariant. The Wightman functions for these two scenarios are similar, except in nonstationary configurations they possess an additional term that breaks time-translation invariance. In section 4.2.1 we focus on a single detector following the four trajectories to examine its transition probability (or response function). We study its dependence on the magnitudes of the acceleration and torsions, and numerically evaluate the effective temperature of the detector. We then consider the correlation harvesting protocol in section 4.2.2. Specifically, concurrence of entanglement and quantum mutual information – which measures the harvested total correlations – are numerically evaluated. We find that the stationary and nonstationary configurations behave in a similar manner since their Wightman functions have terms in common. However, the amount of correlations extracted by the detectors in the nonstationary configurations differs from those of the stationary ones due to an additional term in the Wightman function. We also look into the acceleration dependence of the harvested correlations and conclude that sufficiently high accelerations prevent *any* uniformly accelerating detectors from extracting correlations. This point is consistent with previous papers that focused on linear and circular motions

[56, 38, 57, 58, 55, 44, 59]. Finally, we show that constant acceleration makes it challenging to extract 'genuine entanglement' (entanglement preexistent in a quantum field that has no possible assistance from detector communication) in section 4.2.3. In general, genuine entanglement harvesting can be harvested from causally disconnected spacetime regions due to microcausality. For inertial detectors with Gaussian switching in Minkowski spacetime, it is shown that a sufficiently large energy gap allows the detectors to extract genuine entanglement from such regions [31, 60]. While we find that this is generally not the case for uniformly accelerated detectors, remarkably we find small but non-negligible regions of parameter space where detectors in causal contact can harvest genuine entanglement. All the background is included in chapter 2. We also conclude our overall results and include suggestions for future research in chapter 5.

Throughout this thesis we use the units $\hbar = k_{\mathrm{B}} = c = 1$ and the signature $(-,+,+,+)$, as well as $\mathsf{x} := x^{\mu}$, an event in coordinates x^{μ}.

Chapter 2

Particle detectors in curved spacetime

In this chapter we review the theory of Quantum Field (QFT) in curvred spacetime based on [61][11]

2.1 Quantum Field in curved spacetime

Quantum field theory in curved spacetime is an essential extension of quantum field theory in flat spacetime, paving the way to investigate quantum effects in the presence of gravity. In this framework, the underlying spacetime is treated as a fixed curved background, not subject to quantum fluctuations.

2.1.1 Formulation

The formulation of quantum field theory in curved spacetime requires the incorporation of the principles of general relativity with quantum mechanics. We will discuss the most common scenario, namely a scalar field propagating on a curved manifold.

Consider a classical real scalar field (i.e., Klein-Gordon field), $\phi(\mathsf{x})$, where x is a point in a manifold: $\mathsf{x} \in \mathcal{M}$. The action $S_\phi[\phi, g]$, for this classical scalar field is given by

$$S_\phi[\phi, g] = \frac{1}{2}\sqrt{-g}\int_{\mathcal{M}} \left[\partial_\mu\phi(\mathsf{x})\partial_\nu\phi(\mathsf{x}) - (m^2 + \xi R(\mathsf{x}))\phi^2(\mathsf{x})\right] , \tag{2.1}$$

where g is the determinant of the metric $g_{\mu\nu}$ of the spacetime where the field exists, $m \geq 0$ is the mass of the field, $\xi \in \mathbb{R}$ is a constant describing a coupling between the field and the Ricci scalar $R(\mathsf{x})$, which is the trace of Ricci curvature tensor:

$$R_{\alpha\beta} = \partial_\rho \Gamma^\rho{}_{\beta\alpha} - \partial_\beta \Gamma^\rho{}_{\rho\alpha} + \Gamma^\rho{}_{\rho\lambda}\Gamma^\lambda{}_{\beta\alpha} - \Gamma^\rho{}_{\beta\lambda}\Gamma^\lambda{}_{\rho\alpha} \tag{2.2}$$

where $\Gamma^\lambda_{\mu\nu}$ is the Christoffel symbol given by:

$$\Gamma^\lambda{}_{\mu\nu} = \frac{1}{2} g^{\lambda\rho} \left(\partial_\mu g_{\nu\rho} + \partial_\nu g_{\mu\rho} - \partial_\rho g_{\mu\nu} \right). \tag{2.3}$$

The parameter ξ in the given action for the scalar field describes the coupling between the field and the Ricci scalar $R(\mathbf{x})$. Two particular values of ξ that are often considered in physics correspond to distinct scenarios:

1. **Minimal Coupling**: Minimal coupling corresponds to $\xi = 0$. In this case the scalar field is not coupled to the curvature of spacetime; the equation of motion for the scalar field will be the standard Klein-Gordon equation without any extra terms involving the curvature.

2. **Conformally Coupled Case:** The conformally coupled case in $(n+1)$-dimensional spacetime corresponds to $\xi = (n-1)/4n$. This special value leads to a particular interaction between the field and the curvature that preserves the conformal symmetry of the action. In other words, if the metric is rescaled by a conformal factor (i.e., $g_{\mu\nu} \to \Omega^2 g_{\mu\nu}$ for some positive function Ω), the action for a massless scalar field remains invariant under this transformation.

Action and Equations of Motion

The equations of motion are obtained from the principle of stationary action, leading to the Klein-Gordon equation:

$$(\Box - m^2 - \xi R)\phi(\mathsf{x}) = 0\,, \tag{2.4}$$

where

$$\Box \coloneqq \frac{1}{\sqrt{-g}} \partial_\mu (g^{\mu\nu} \sqrt{-g} \partial_\nu) \tag{2.5}$$

is the d'Alembert operator. The Klein-Gordon equation mainly depends on the spacetime geometry.

2.1.2 Quantization

Mode Expansion

The quantization process starts by expanding the field in terms of modes that satisfy the curved-space Klein-Gordon equation given in 2.4. These modes $u_k(x)$ are chosen to respect the manifold's geometry:

$$\hat{\phi}(\mathsf{x}) = \int_{\mathbb{R}^n} \mathrm{d}^n k \, \left(\hat{a}_{\boldsymbol{k}} u_{\boldsymbol{k}}(\mathsf{x}) + \hat{a}^\dagger_{\boldsymbol{k}} u^*_{\boldsymbol{k}}(\mathsf{x}) \right) . \tag{2.6}$$

where $u_{\boldsymbol{k}}(\mathsf{x}) \in \mathbb{C}$ is the mode function. a_k and $a_k^\dagger$ are the annihilation and creation operators satisfying the canonical commutation relations.
$[a_i, a_j^\dagger] = \delta_{ij} \quad \text{and} \quad [a_i, a_j] = [a_i^\dagger; a_j^\dagger] = 0$

In the Minkowski coordinates (t, x, y, z), the mode function reads

$$u_{\boldsymbol{k}}(\mathsf{x}) = \frac{1}{\sqrt{(2\pi)^3 2\omega_{\boldsymbol{k}}}} e^{-\mathrm{i}\omega_{\boldsymbol{k}} t + \mathrm{i}\boldsymbol{k}\cdot\boldsymbol{x}} , \tag{2.7}$$

where $\omega_{\boldsymbol{k}} = \sqrt{|\boldsymbol{k}|^2 + m^2}$ with m being the mass of the scalar field. Therefore, the mode decomposition is

$$\hat{\phi}(\mathsf{x}) = \int_{\mathbb{R}^3} \frac{\mathrm{d}^3 k}{\sqrt{(2\pi)^3 2\omega_{\boldsymbol{k}}}} \left(\hat{a}_{\boldsymbol{k}} e^{-\mathrm{i}\omega_{\boldsymbol{k}} t + \mathrm{i}\boldsymbol{k}\cdot\boldsymbol{x}} + \hat{a}^\dagger_{\boldsymbol{k}} e^{\mathrm{i}\omega_{\boldsymbol{k}} t - \mathrm{i}\boldsymbol{k}\cdot\boldsymbol{x}} \right) , \tag{2.8}$$

and the Minkowski vacuum $|0_{\mathrm{M}}\rangle$ is defined as $\hat{a}_{\boldsymbol{k}} |0_{\mathrm{M}}\rangle = 0$ for all $\boldsymbol{k}$.

Correlation Functions

Let ρ_ϕ be the quantum state of the field, the two point correlation function of this state (Wightman function) is defined as the following:

$$W(\mathsf{x}, \mathsf{x}') = \langle \hat{\phi}(\mathsf{x}) \hat{\phi}(\mathsf{x}') \rangle_{\rho_\phi} , \tag{2.9}$$

The Wightman function satisfies the Klein-Gordon equation Eq.2.4

$$(\Box - m^2 - \xi R) W(x, x') = 0 , \tag{2.10}$$

If the field is in vacuum state, the Wightman function reads
$W(\mathsf{x},\mathsf{x}') = \langle 0|\hat{\phi}(\mathsf{x})\hat{\phi}(\mathsf{x}')|0\rangle$

In the case of Minkowski coordinates (t, x, y, z), using the mode decomposition in Eq. 2.8 the Wightman function in the Minkowski vacuum state reads

$$W(\mathsf{x},\mathsf{x}') = -\frac{1}{4\pi^2}\frac{1}{(t-t'-\mathsf{i}\epsilon)^2 - |\boldsymbol{x}-\boldsymbol{x}'|^2}\,, \tag{2.11}$$

where ϵ is a UV regulator.
The Wightman function can be decomposed into two parts (commutator, and anti-commutator) defined as the following:

$$W(\mathsf{x},\mathsf{x}') = \mathrm{Re}[W(\mathsf{x},\mathsf{x}')] + \mathsf{i}\ \mathrm{Im}[W(\mathsf{x},\mathsf{x}')] \tag{2.12}$$

Where

$$\mathrm{Re}[W(\mathsf{x},\mathsf{x}')] = \frac{1}{2}\langle 0|\{\hat{\phi}(\mathsf{x}),\hat{\phi}(\mathsf{x}')\}|0\rangle\ , \tag{2.13}$$

$$\mathrm{Im}[W(\mathsf{x},\mathsf{x}')] = \frac{-\mathsf{i}}{2}[\hat{\phi}(\mathsf{x}),\hat{\phi}(\mathsf{x}')]\,. \tag{2.14}$$

2.1.3 KMS State

The Kubo-Martin-Schwinger (KMS) state [62, 63] is a generalization of Gibbs thermal state defined as

$$\rho_{\mathrm{th}} = \frac{1}{Z}e^{-\beta\hat{H}}\,, \tag{2.15}$$

where:
$Z = \mathrm{Tr}[e^{-\beta\hat{H}}]$, $\beta = \dfrac{1}{T}$, and $\hat{H}$ is the Hamiltonian of the bath.
This definition presents challenges in the context of quantum fields due to non-separability of the Hilbert space. Since the basis in the Hilbert space of a field is uncountable, a trace may be ill-defined. The KMS state generalizes the Gibbs state to non-separable Hilbert spaces.

If the field is in the KMS thermal state with respect to time τ at the inverse KMS temperature $\beta_{\rm KMS}$, then the Wightman function satisfies

$$W(\Delta\tau - \mathrm{i}\beta_{\rm KMS}) = W(-\Delta\tau)\,, \tag{2.16}$$

where $\Delta\tau \coloneqq \tau - \tau'$. The Wightman function in this case would be time translation invariant with respect to τ.

2.2 The Unruh Dewitt particle detectors in a quantum field

The Unruh-DeWitt particle detector (UDW), named after physicists William G. Unruh and Bryce S. DeWitt, is a theoretical construct in quantum field theory. It is used in the context of thought experiments to investigate the phenomenon of particle detection by accelerating observers or observers in gravitational fields, taking into account the principles of quantum field theory. The Unruh effect [1] proposes that an observer who is constantly accelerating in empty space would perceive the vacuum of that space as being populated with particles. In other words, this observer would interpret the vacuum as having a non-zero temperature and emitting particles. The Unruh-DeWitt detector is typically modeled as a two-level quantum system that can be considered as a qubit locally coupled to a quantum field. We denote the ground and excited states for detector-$j \in \{\mathrm{A}, \mathrm{B}\}$ by $|g_j\rangle$ and $|e_j\rangle$, respectively, with the energy gap Ω_j between them in the detector's reference frame. The detector can transition between these states when it interacts with a particle from the field. By studying the transition probabilities and the response of the detector as it accelerates or is subjected to a gravitational field, we can gain insights into how the observer's perception of particles is affected by these conditions.

2.2.1 Single UDW detector

Consider a detector D, with ground and excited states $|g_D\rangle$ and $|e_D\rangle$, respectively, whose energy gap is Ω_D. These states form an orthonormal basis for the Hilbert space $\mathcal{H}_D \otimes \mathbb{C}^2$ associated with internal degrees of freedom of the detector. The free evolution of this detector is governed by the Hamiltonian

$$H_0 = \frac{\Omega}{2}\left(|e\rangle_D\langle e|_D - |g\rangle_D\langle g|_D\right), \tag{2.17}$$

The detector's interaction with a scalar field $\phi(x)$ is described by

$$\hat{H}_{D,\text{int}} = \lambda\chi(\tau)(\hat{\sigma}^+ + \hat{\sigma}^-) \otimes \hat{\phi}(x(\tau)) \tag{2.18}$$

where $\chi(\tau) \in [0,1]$ is the switching function, that controls the duration of the detector's interaction with the field, λ is the interaction strength, and $\hat{\sigma}^+ \equiv |e\rangle\langle g|$ and $\hat{\sigma}^- \equiv |g\rangle\langle e|$ are the raising and lowering operators, respectively, acting on the Hilbert space of the UDW detector. $\hat{\phi}(\mathsf{x}(\tau))$ is the field operator along the detector's trajectory. In this sense, the detector locally couples to the field at the point where it is located. The time evolution of the detector and the field during the interaction process,is described by the unitary operator generated by the interaction Hamiltonian in Eq (2.17)

$$U := \mathcal{T}\exp\left(-i\int d\tau\, H_D(\tau)\right) = 1 - i\int d\tau\, H_D(\tau) + \frac{(-i)^2}{2}\int d\tau\, d\tau'\, \mathcal{T}H_D(\tau)H_D(\tau') + \mathcal{O}(\lambda^3) \tag{2.19}$$

where $\tau \in (-\infty;\infty)$ and $\mathcal{T}$ is the time ordering operator defined as

$$\mathcal{T}[A(t)B(t')] := \theta(t-t')A(t)B(t') + \theta(t'-t)B(t')A(t)\ .$$

Applying the time evolution operator on the system where the detector and the field are both prepared in ground state $|g_D\rangle|0\rangle$, we get the final state of the system after the interaction as the following:

$$\begin{aligned} U|g_D\rangle|0\rangle &= \left(1 - i\int d\tau\, H_D(\tau) - \frac{1}{2}\int d\tau\, d\tau'\, \mathcal{T}H_D(\tau)H_D(\tau') + \mathcal{O}(\lambda)\right)|g\rangle_D|0\rangle \\ &= |g_D\rangle|0\rangle - i\lambda\int d\tau\, \chi_D(\tau)e^{i\Omega_D\tau}|e_D\rangle \otimes \phi[x_D(\tau)]|0\rangle \\ &\quad - \frac{\lambda^2}{2}\int d\tau\, d\tau'\, \chi_D(\tau)\chi_D(\tau')\mathcal{T}[\hat{\sigma}^-(\tau)\hat{\sigma}^+(\tau') + \hat{\sigma}^+(\tau)\hat{\sigma}^-(\tau')]|g_D\rangle \\ &\quad \otimes \mathcal{T}\phi[x_D(\tau)]\phi[x_D(\tau')]|g\rangle + \mathcal{O}(\lambda^3) \end{aligned} \tag{2.20}$$

we can get the final state of the detector D by tracing over the field degrees of freedom in Eq. (2.20):

$$\rho_D := \text{tr}_\phi\left(U|0\rangle\langle 0| \otimes |g_D\rangle\langle g_D|U^\dagger\right) = \begin{pmatrix} 1-\mathcal{L}_D & 0 \\ 0 & \mathcal{L}_D \end{pmatrix} + \mathcal{O}(\lambda^4). \tag{2.21}$$

where ρ_D is the detector's density matrix in the basis $\{|g_D\rangle, |e_D\rangle\}$ and $\mathcal{L}_\mathcal{D}$ is the probability that the detector has transitioned from ground to excited state during the interaction given by

$$\mathcal{L}_D = \lambda^2\int_{\mathbb{R}} \mathrm{d}\tau \int_{\mathbb{R}} \mathrm{d}\tau'\, \chi_D(\tau)\chi_D(\tau')e^{-\mathrm{i}\Omega(\tau-\tau')} \times W\left(\mathsf{x}_D(\tau), \mathsf{x}_D(\tau')\right), \tag{2.22}$$

and $W(x,x')$ is the vacuum Wightman function:

$$W(x,x') := \langle 0|\phi(x)\phi(x')|0\rangle \tag{2.23}$$

2.2.2 Two UDW detectors

Let us introduce two UDW particle detectors A and B that interact with a quantum scalar field $\hat{\phi}$. The dynamics of the detectors is governed by a Hamiltonian. Assuming the size of the detectors is negligible and each detector has its own proper time τ_j, the interaction Hamiltonian in the interaction picture is given by

$$\hat{H}_j^{\tau_j}(\tau_j) = \lambda_j \chi_j(\tau_j)\hat{\mu}_j(\tau_j) \otimes \hat{\phi}(\mathsf{x}_j(\tau_j))\,.\; j \in \{\mathrm{A},\mathrm{B}\} \tag{2.24}$$

The operator $\hat{\mu}_j(\tau_j)$ is the monopole moment, which describes the internal dynamics of each detector given by

$$\hat{\mu}_j(\tau_j) = |e_j\rangle\langle g_j|\, e^{\mathsf{i}\Omega_j\tau_j} + |g_j\rangle\langle e_j|\, e^{-\mathsf{i}\Omega_j\tau_j}\,. \tag{2.25}$$

The superscript on the Hamiltonian $\hat{H}_j^{\tau_j}(\tau_j)$ indicates that it is the generator of time-translation with respect to the proper time τ_j.

The total interaction Hamiltonian, $\hat{H}_{\mathrm{I}}^t(t)$, that describes both detectors A and B is then given by

$$\hat{H}_{\mathrm{I}}^t(t) = \frac{\mathrm{d}\tau_{\mathrm{A}}}{\mathrm{d}t}\hat{H}_{\mathrm{A}}^{\tau_{\mathrm{A}}}\Big(\tau_{\mathrm{A}}(t)\Big) + \frac{\mathrm{d}\tau_{\mathrm{B}}}{\mathrm{d}t}\hat{H}_{\mathrm{B}}^{\tau_{\mathrm{B}}}\Big(\tau_{\mathrm{B}}(t)\Big)\,, \tag{2.26}$$

where the Hamiltonian $\hat{H}_{\mathrm{I}}^t(t)$ is now a generator of time-translation with respect to the common time t (e.g., Minkowski time). Similar to a single detector, the time-evolution operator $\hat{U}_{\mathrm{I}}$ can be written by using a time-ordering symbol $\mathcal{T}_t$ with respect to t [64, 65]:

$$\hat{U}_{\mathrm{I}} = \mathcal{T}_t \exp\left(-\mathsf{i}\int_{\mathbb{R}} \mathrm{d}t\, \hat{H}_{\mathrm{I}}^t(t)\right). \tag{2.27}$$

Assuming that the coupling strength λ is small, the Dyson series expansion of $\hat{U}_{\mathrm{I}}$ reads:

$$\hat{U}_{\mathrm{I}} = \mathbb{1} + \hat{U}_{\mathrm{I}}^{(1)} + \hat{U}_{\mathrm{I}}^{(2)} + \mathcal{O}(\lambda^3)\,, \tag{2.28a}$$

$$\hat{U}_{\mathrm{I}}^{(1)} = -\mathsf{i}\int_{-\infty}^{\infty} \mathrm{d}t\, \hat{H}_{\mathrm{I}}^t(t)\,, \tag{2.28b}$$

$$\hat{U}_{\mathrm{I}}^{(2)} = -\int_{-\infty}^{\infty}\mathrm{d}t_1 \int_{-\infty}^{t_1}\mathrm{d}t_2\, \hat{H}_{\mathrm{I}}^t(t_1)\hat{H}_{\mathrm{I}}^t(t_2)\,. \tag{2.28c}$$

Let us now obtain the density matrix for the detectors up to the second order in λ. We assume that the initial states of the detectors and the field are in the ground $|g_{\rm A}\rangle \otimes |g_{\rm B}\rangle$ and vacuum $|0\rangle$ states respectively, and uncorrelated. The rationale for this assumption is twofold. First, it is a natural assumption to make in the lab, as it is straightforward to initialize systems to be in their ground states. Second, this assumption allows us to study harvesting of vacuum correlations without contaminants from other sources. It is certainly possible to relax the assumption of an initially uncorrelated state, and recently studies of entanglement harvesting in this context have been carried out [66, 67].

We therefore take the initial state ρ_0 of the total system to be

$$\rho_0 = |g_{\rm A}\rangle\langle g_{\rm A}| \otimes |g_{\rm B}\rangle\langle g_{\rm B}| \otimes |0\rangle\langle 0| \ . \tag{2.29}$$

The final total density matrix $\rho_{\rm tot}$ after the interaction reads

$$\begin{aligned}\rho_{\rm tot} &= \hat{U}_{\rm I}\rho_0\hat{U}_{\rm I}^\dagger \\ &= \rho_0 + \rho^{(1,1)} + \rho^{(2,0)} + \rho^{(0,2)} + \mathcal{O}(\lambda^4)\,,\end{aligned} \tag{2.30}$$

where $\rho^{(i,j)} = \hat{U}^{(i)}\rho_0\hat{U}^{(j)\dagger}$. Note that all the odd-power terms of λ vanish [31], in the final density matrix of the detectors upon tracing out the field degree of freedom: $\rho_{\rm AB} = {\rm Tr}_\phi[\rho_{\rm tot}]$. In the basis $\{|g_{\rm A}g_{\rm B}\rangle, |g_{\rm A}e_{\rm B}\rangle, |e_{\rm A}g_{\rm B}\rangle, |e_{\rm A}e_{\rm B}\rangle\}$, $\rho_{\rm AB}$ is known to be

$$\rho_{\rm AB} = \begin{bmatrix} 1-\mathcal{L}_{\rm AA}-\mathcal{L}_{\rm BB} & 0 & 0 & \mathcal{M}^* \\ 0 & \mathcal{L}_{\rm BB} & \mathcal{L}_{\rm AB}^* & 0 \\ 0 & \mathcal{L}_{\rm AB} & \mathcal{L}_{\rm AA} & 0 \\ \mathcal{M} & 0 & 0 & 0 \end{bmatrix} + \mathcal{O}(\lambda^4) \tag{2.31}$$

where

$$\mathcal{L}_{ij} = \lambda^2 \int_{\mathbb{R}} {\rm d}\tau_i \int_{\mathbb{R}} {\rm d}\tau_j'\, \chi_i(\tau_i)\chi_j(\tau_j') e^{-{\rm i}\Omega(\tau_i-\tau_j')} W\Big(\mathsf{x}_i(\tau_i), \mathsf{x}_j(\tau_j')\Big)\,, \tag{2.32a}$$

$$\begin{aligned}\mathcal{M} = -\lambda^2 &\int_{\mathbb{R}} {\rm d}\tau_{\rm A} \int_{\mathbb{R}} {\rm d}\tau_{\rm B}\, \chi_{\rm A}(\tau_{\rm A})\chi_{\rm B}(\tau_{\rm B}) e^{-{\rm i}\Omega(\tau_{\rm A}+\tau_{\rm B})} \\ &\times \Big[\Theta\Big(t(\tau_{\rm A}) - t(\tau_{\rm B})\Big) W\Big(\mathsf{x}_{\rm A}(\tau_{\rm A}), \mathsf{x}_{\rm B}(\tau_{\rm B})\Big) \\ &\quad + \Theta\Big(t(\tau_{\rm B}) - t(\tau_{\rm A})\Big) W\Big(\mathsf{x}_{\rm B}(\tau_{\rm B}), \mathsf{x}_{\rm A}(\tau_{\rm A})\Big)\Big]\,,\end{aligned} \tag{2.32b}$$

where $\Theta(t)$ is the Heaviside step function and $W(\mathsf{x},\mathsf{y}) \coloneqq \langle 0|\,\hat{\phi}(\mathsf{x})\hat{\phi}(\mathsf{y})\,|0\rangle$ is the Wightman function. The elements $\mathcal{L}_{jj}$, $j \in \{{\rm A}, {\rm B}\}$ are the transition probabilities (or responses) from the ground $|g_j\rangle$ to excited $|e_j\rangle$ states. The off-diagonal elements $\mathcal{M}$ and $\mathcal{L}_{\rm AB}$ contribute to entanglement and mutual information, respectively.

2.3 Correlation Harvesting in curved spacetime

We introduce two measures for correlation: concurrence $\mathcal{C}$, and quantum mutual information $I_{\rm AB}$.

2.3.1 Concurrence as a measure of entanglement

Concurrence of entanglement [68, 69] is a measure of entanglement. Let $\rho_{\rm AB}$ be the density matrix of a two-qubit system. We first define a matrix $\tilde{\rho}_{\rm AB}$ as

$$\tilde{\rho}_{\rm AB} \coloneqq (\hat{\sigma}_y \otimes \hat{\sigma}_y)\rho^*_{\rm AB}(\hat{\sigma}_y \otimes \hat{\sigma}_y)\,, \tag{2.33}$$

where $\hat{\sigma}_y$ is the Pauli-y operator and $\rho^*_{\rm AB}$ is a complex conjugate of $\rho_{\rm AB}$. Then by denoting $w_i \in \mathbb{R}$, $(i = 1, 2, 3, 4)$ as eigenvalues of a Hermitian operator $\sqrt{\sqrt{\rho_{\rm AB}}\tilde{\rho}_{\rm AB}\sqrt{\rho_{\rm AB}}}$, the concurrence is defined as follows.

$$\mathcal{C} \coloneqq \max\{0,\, w_1 - w_2 - w_3 - w_4\}\,, (w_1 \geq w_2 \geq w_3 \geq w_4). \tag{2.34}$$

The concurrence is zero if and only if the state $\rho_{\rm AB}$ is separable. In the case of our density matrix (2.31), the concurrence is known to be

$$\mathcal{C} = 2\max\{0,\, |\mathcal{M}| - \sqrt{\mathcal{L}_{\rm AA}\mathcal{L}_{\rm BB}}\} + \mathcal{O}(\lambda^4)\,. \tag{2.35}$$

2.3.2 Quantum Mutual information as a measure of total correlation

Quantum mutual information [70] quantifies the amount of total correlation including both classical and quantum. Mutual information $I_{\rm AB}$ between detectors A and B up to second order in λ is [31]

$$I_{\rm AB} = \mathcal{L}_+ \ln \mathcal{L}_+ + \mathcal{L}_- \ln \mathcal{L}_- - \mathcal{L}_{\rm AA} \ln \mathcal{L}_{\rm AA} - \mathcal{L}_{\rm BB} \ln \mathcal{L}_{\rm BB} + \mathcal{O}(\lambda^4)\,, \tag{2.36}$$

where

$$\mathcal{L}_\pm \coloneqq \frac{1}{2}\left(\mathcal{L}_{\rm AA} + \mathcal{L}_{\rm BB} \pm \sqrt{(\mathcal{L}_{\rm AA} - \mathcal{L}_{\rm BB})^2 + 4|\mathcal{L}_{\rm AB}|^2}\right). \tag{2.37}$$

and $\mathcal{L}_{\rm ij}$ is defined in Eq (2.32a).
Note that, while concurrence (2.35) vanishes when the "noise term" $\sqrt{\mathcal{L}_{\rm AA}\mathcal{L}_{\rm BB}}$ exceeds the

nonlocal element $|\mathcal{M}|$, the mutual information becomes zero when $|\mathcal{L}_{\rm AB}| = 0$. In particular, from the condition $\mathcal{L}_{\rm AA}\mathcal{L}_{\rm BB} \geq |\mathcal{L}_{\rm AB}|^2$ [32], if one of the transition probabilities satisfies $\mathcal{L}_{jj} = 0$ then $|\mathcal{L}_{\rm AB}| = 0$, thereby $I_{\rm AB} = 0$. In addition, if $\mathcal{C} = 0$ but the mutual information is nonvanishing, then the extracted correlation by the detectors is either classical correlation or nondistillable entanglement.

Throughout this thesis, we shall use a Gaussian switching function

$$\chi_j(\tau_j) = e^{-\tau_j^2/2\sigma^2}\,, \tag{2.38}$$

which is a particular function in the set of single-peaked rapidly decreasing functions. This function allows for considerable analytic simplification in the elements of the density matrix.

Chapter 3

Correlation Harvesting of uniformly accelerating particle detectors in linear motion

In this chapter, we study the mutual information harvesting protocol of two UDW particle detectors uniformly accelerated in linear motion. Through numerical analysis, we demonstrate that a single detector exhibits behavior similar to that of being immersed in a thermal bath. However, when considering the quantum mutual information between two accelerating detectors, it differs from that observed between two inertial detectors in a thermal bath. This distinction arises due to the fact that while the Wightman function along the trajectory of a single uniformly accelerating detector matches that of a detector in a thermal bath, a pair of detectors in the same respective scenarios exhibit different Wightman functions. Furthermore, we note a qualitative similarity in the behavior of harvested quantum mutual information and harvested entanglement. Both measures are enhanced at lower temperatures but decrease as the Unruh temperature increases.

The chapter is structured as follows. First, we establish the trajectories of the detectors, considering three configurations of accelerating detector pairs—parallel, anti-parallel, and perpendicular [55]. Second, we calculate mutual information harvesting and entanglement harvesting with varying the acceleration. Last, we discuss the results and compare them to previous studies.

3.0.1 Detectors' trajectories

We will focus on uniformly accelerating detectors in $(3+1)$-dimensional Minkowski spacetime. Specifically, we utilize a massless quantum scalar field $\hat{\phi}(\mathsf{x})$ that obeys the Klein-Gordon equation Eq. 2.4 and with assuming that the field is minimally coupled. As mentioned in 2.1.2:

$$\hat{\phi}(\mathsf{x}) = \int \frac{\mathrm{d}^3 k}{\sqrt{(2\pi)^3 2|\boldsymbol{k}|}} \left(\hat{a}_{\boldsymbol{k}} e^{-\mathrm{i}|\boldsymbol{k}|t + \mathrm{i}\boldsymbol{k}\cdot\boldsymbol{x}} + \text{h.c.}\right) , \tag{3.1}$$

with the Minkowski vacuum $|0\rangle$ satisfying $\hat{a}_{\boldsymbol{k}}|0\rangle = 0$ for all $\boldsymbol{k}$. The creation and annihilation operators obey the canonical commutation relations,

$$[\hat{a}_{\boldsymbol{k}}, \hat{a}^\dagger_{\boldsymbol{k}'}] = \delta^{(3)}(\boldsymbol{k} - \boldsymbol{k}') , \tag{3.2a}$$

$$[\hat{a}_{\boldsymbol{k}}, \hat{a}_{\boldsymbol{k}'}] = 0 , \quad [\hat{a}^\dagger_{\boldsymbol{k}}, \hat{a}^\dagger_{\boldsymbol{k}'}] = 0 . \tag{3.2b}$$

Then the Wightman function in the Minkowski vacuum state $|0\rangle$ satisfying $\hat{a}_{\boldsymbol{k}}|0\rangle = 0$ for all $\boldsymbol{k}$ is known to be

$$W(\mathsf{x}, \mathsf{x}') = -\frac{1}{4\pi^2} \frac{1}{(t - t' - \mathrm{i}\epsilon)^2 - |\boldsymbol{x} - \boldsymbol{x}'|^2} , \tag{3.3}$$

where ϵ is a UV regulator.

To evaluate the elements in the density matrix ρ_{AB} (2.31), one needs to specify the trajectories of detectors A and B in this Wightman function. In what follows, we will consider three different acceleration scenarios: parallel, anti-parallel, and perpendicular.

Parallel acceleration

In this scenario, a pair of UDW detectors A and B are accelerating in the same direction along x axis, with separation L between them at all times, as shown in Fig. 3.1(a). The detectors' trajectories can be written as

$$\mathsf{x}_{\mathrm{A}} = \left\{ t = \frac{1}{a}\sinh(a\tau_{\mathrm{A}}), x = \frac{1}{a}[\cosh(a\tau_{\mathrm{A}}) - 1] + \frac{L}{2}, y = z = 0 \right\} , \tag{3.4}$$

$$\mathsf{x}_{\mathrm{B}} = \left\{ t = \frac{1}{a}\sinh(a\tau_{\mathrm{B}}), x = \frac{1}{a}[\cosh(a\tau_{\mathrm{B}}) - 1] - \frac{L}{2}, y = z = 0 \right\} . \tag{3.5}$$

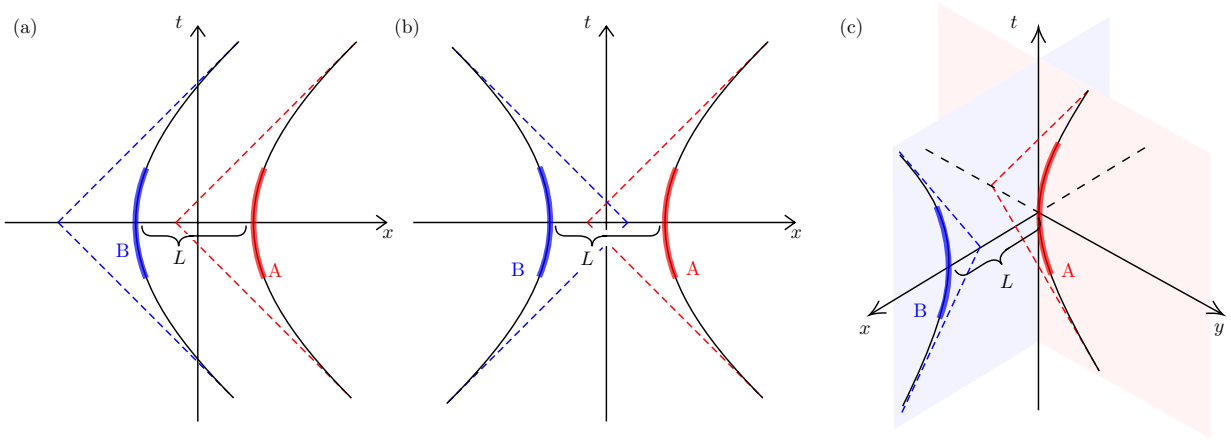

Figure 3.1: Three configurations of acceleration: (a) parallel, (b) anti-parallel, and (c) perpendicular. The red and blue stripes indicate the interaction duration of detectors A and B, respectively. In all cases, the detectors are separated by L at $t = 0$, at which their Gaussian switching peaks. Note that the separation in the parallel configuration is L for all times.

By substituting these trajectories into the Wightman function (3.3), we can evaluate the elements in the density matrix (2.31) along the trajectories. The Wightman function $W_a(\mathsf{x}, \mathsf{y})$ becomes

$$W_a(\mathsf{x}_j(\tau_j), \mathsf{x}'_j(\tau'_j)) = -\frac{a^2}{16\pi^2} \frac{1}{\sinh^2[a(\tau_j - \tau'_j)/2 - \mathrm{i}\epsilon]}, \quad j \in \{\mathrm{A}, \mathrm{B}\} \tag{3.6}$$

$$W_a(\mathsf{x}_\mathrm{A}(\tau_\mathrm{A}), \mathsf{x}_\mathrm{B}(\tau_\mathrm{B})) = -\frac{a^2}{4\pi^2} \frac{1}{[\sinh(a\tau_\mathrm{A}) - \sinh(a\tau_\mathrm{B}) - \mathrm{i}\epsilon]^2 - |\cosh(a\tau_\mathrm{A}) - \cosh(a\tau_\mathrm{B}) + aL|^2}. \tag{3.7}$$

The transition probability $\mathcal{L}_{jj}$ can be simplified to [55]

$$\mathcal{L}_{jj} = \frac{\lambda^2}{4\pi}[e^{-\Omega^2\sigma^2} - \sqrt{\pi}\Omega\sigma\mathrm{erfc}(\Omega\sigma)] + \frac{\lambda^2 a\sigma}{4\pi^{3/2}} \int_0^\infty \mathrm{d}s \, \frac{\cos(\beta s) e^{-\alpha s^2} (\sinh^2 s - s^2)}{s^2 \sinh^2 s}, \tag{3.8}$$

where $\beta \equiv 2\Omega/a$ and $\alpha \equiv 1/(a\sigma)^2$. $\mathrm{erfc}(x) \coloneqq 1 - \mathrm{erf}(x)$ is the complementary error function, where

$$\mathrm{erf}(x) \coloneqq \frac{2}{\sqrt{\pi}} \int_0^x \mathrm{d}s \, e^{-s^2} \tag{3.9}$$

is the error function. The switching function is Gaussian switching (2.38).

Note that the first term in $\mathcal{L}_{jj}$ is the transition probability of a detector at rest in $(3+1)$-dimensional Minkowski spacetime and the transition rate for the two detectors A and B is identical as they have the same spatial translation.

Anti-parallel acceleration

The anti-parallel configuration, shown in Fig. 3.1(b), is the case where two detectors accelerate towards each other and after momentarily stopping (at which point the detector separation is L), they accelerate away. Unlike the parallel acceleration configuration, the distance between the detectors is not fixed.

The trajectories are given by

$$\mathsf{x}_{\mathrm{A}} = \left\{ t = \frac{1}{a}\sinh(a\tau_{\mathrm{A}}), x = \frac{1}{a}[\cosh(a\tau_{\mathrm{A}}) - 1] + \frac{L}{2}, y = z = 0 \right\}, \tag{3.10}$$

$$\mathsf{x}_{\mathrm{B}} = \left\{ t = \frac{1}{a}\sinh(a\tau_{\mathrm{B}}), x = \frac{-1}{a}[\cosh(a\tau_{\mathrm{B}}) - 1] - \frac{L}{2}, y = z = 0 \right\}. \tag{3.11}$$

This yields the following Wightman function:

$$W_a(\mathsf{x}_{\mathrm{A}}(\tau_{\mathrm{A}}), \mathsf{x}_{\mathrm{B}}(\tau_{\mathrm{B}})) = -\frac{1}{4\pi^2} \frac{1}{\left[\frac{1}{a}\sinh a\tau_A - \frac{1}{a}\sinh a\tau_B - \mathsf{i}\epsilon\right]^2 - \left[\frac{1}{a}\cosh a\tau_A - \frac{1}{a} + \frac{L}{2} - \left(-\frac{1}{a}\cosh a\tau_B + \frac{1}{a} - \frac{L}{2}\right)\right]^2}$$

While the Wightman function along both the trajectories, $W(\mathsf{x}_{\mathrm{A}}, \mathsf{x}_{\mathrm{B}})$, differs from (3.7) and therefore $\mathcal{L}_{\mathrm{AB}}$ and $\mathcal{M}$ in the density matrix also differ from the parallel case (2.31), the transition probability $\mathcal{L}_{jj}$ is the same as (3.8). Note that the detectors, as long as L is small, can in general communicate with each other by exchanging field quanta when the detectors are lightlike separated.

Perpendicular acceleration

As depicted in Fig. 3.1(c), the perpendicular acceleration configuration is similar to the anti-parallel configuration, but now detectors are traveling along different axes x and y.

That is, the two detectors accelerate toward and away from each other along linear trajectories at a 90° angle. The minimum distance between them at which they stop momentarily is L. The trajectories are

$$\mathsf{x}_{\mathrm{A}} = \left\{ t = \frac{1}{a}\sinh(a\tau_{\mathrm{A}}), y = \frac{1}{a}[\cosh(a\tau_{\mathrm{A}}) - 1], x = z = 0 \right\}, \tag{3.12}$$

$$\mathsf{x}_{\mathrm{B}} = \left\{ t = \frac{1}{a}\sinh(a\tau_{\mathrm{B}}), x = \frac{1}{a}[\cosh(a\tau_{\mathrm{B}}) - 1] + L, y = z = 0 \right\}. \tag{3.13}$$

In this case the Wightman function reads:

$$W_a(\mathsf{x}_{\mathrm{A}}(\tau_{\mathrm{A}}), \mathsf{x}_{\mathrm{B}}(\tau_{\mathrm{B}})) = \frac{a^2}{4\pi^2\left((-1 + aL + \cosh(a\tau_{\mathrm{B}}))^2 + 4\sinh^4\left(\frac{a\tau_{\mathrm{A}}}{2}\right)\right)} \tag{3.14}$$

Note again that the transition probability $\mathcal{L}_{jj}$ of each detector is the same as (3.8).

3.1 Results

In this section we explore the mutual information harvesting of the two UDW detectors based on the specified trajectories. Notably, we find that increased acceleration negatively affects correlation harvesting. Furthermore, while both the Unruh temperature and the thermal bath temperature exhibit identical response functions for a single detector, their influence on mutual information harvesting diverges. This difference is attributed to their distinct Wightman functions.

3.1.1 Temperature dependence

Figure 3.2 shows the effect of acceleration on mutual information harvesting for each of the scenarios in Fig. 3.1, plotting mutual information I_{AB} as a function of acceleration $a\sigma$ (which is proportional to the Unruh temperature $T_{\mathrm{U}} = a/2\pi$). The diagrams depict different energy gaps Ω and detector separations L at $t = 0$. Figures 3.2(a) and (b) depict I_{AB} with $\Omega\sigma = 0.5$ and 2, respectively, when the separation is small ($L/\sigma = 1$), whereas (c) and (d) have a large separation: $L/\sigma = 7$ for the same two gaps. Note that the effect of communication between the two detectors is negligible when $L/\sigma = 7$, which suggests that the harvested mutual information predominantly comes from preexisting entanglement in the vacuum state of the field.

We see that high acceleration suppresses mutual information harvesting in all three acceleration scenarios regardless of the energy gap $\Omega\sigma$ and separation L/σ. This characteristic property of mutual information can be explained as follows. Since the two detectors have the same transition probabilities, $\mathcal{L}_{\rm AA} = \mathcal{L}_{\rm BB} \equiv P$, then $\mathcal{L}_\pm$ in (2.37) becomes

$$\mathcal{L}_\pm = P \pm |\mathcal{L}_{\rm AB}| \,. \tag{3.15}$$

The reason that $I_{\rm AB}$ vanishes at high acceleration (or equivalently, high temperatures $T_{\rm U} \to \infty$) is that the transition probability P monotonically increases with $a\sigma$ while $|\mathcal{L}_{\rm AB}|$ remains small, which leads to $P \gg |\mathcal{L}_{\rm AB}|$ and so $\mathcal{L}_\pm \approx P$. Thus, the mutual information $I_{\rm AB} \approx 0$. However for a thermal bath (Fig. 1.1) [43], the mutual information between two inertial detectors increases with T because both P and $|\mathcal{L}_{\rm AB}|$ increase with temperature T; consequently the mutual information monotonically increases with T.

By contrast, small acceleration seems to affect mutual information harvesting differently depending on the type of acceleration, energy gap, and detectors' separation. In the case of small energy gap and small detector separation, shown in Fig. 3.2(a), we find that small acceleration enhances mutual information for anti-parallel and perpendicular configurations with higher harvested mutual information in the anti-parallel scenario, while harvested mutual information monotonically decreases with $a\sigma$ in the parallel acceleration case. Nevertheless, as the energy gap $\Omega\sigma$ changes from 0.5 to 2, the acceleration dependence of $I_{\rm AB}$ changes, as shown in Fig. 3.2(b). In particular, the parallel acceleration case no longer monotonically decreases with $a\sigma$, and smaller acceleration could enhance mutual information harvesting. This is also true for $L/\sigma = 7$ in Figs. 3.2(c) and (d). We also examine how harvested mutual information changes with the energy gap by plotting $I_{\rm AB}$ as a function of $\Omega\sigma$ in Fig. 3.3. Here, we fix the value of acceleration to be $a\sigma = 1$, and plot the energy gap dependence when $L/\sigma = 1$ and 7 in Figs. 3.3(a) and (b), respectively. For entanglement harvesting reported in [55], any accelerating detectors (as well as inertial detectors) with small energy gaps cannot extract entanglement when the detector separation L is large. However, this is not the case for mutual information; we find that for both $L/\sigma = 1$ and 7 in Fig. 3.3, mutual information $I_{\rm AB}$ is nonvanishing near $\Omega = 0$, which suggests that the harvested correlation with small Ω is either classical correlation or nondistillable entanglement.

3.1.2 Comparison to previous studies

As we have shown in the previous section, harvested quantum mutual information $I_{\rm AB}$ behaves in a manner similar to harvested entanglement [55]. From Fig. 1.1, we can now

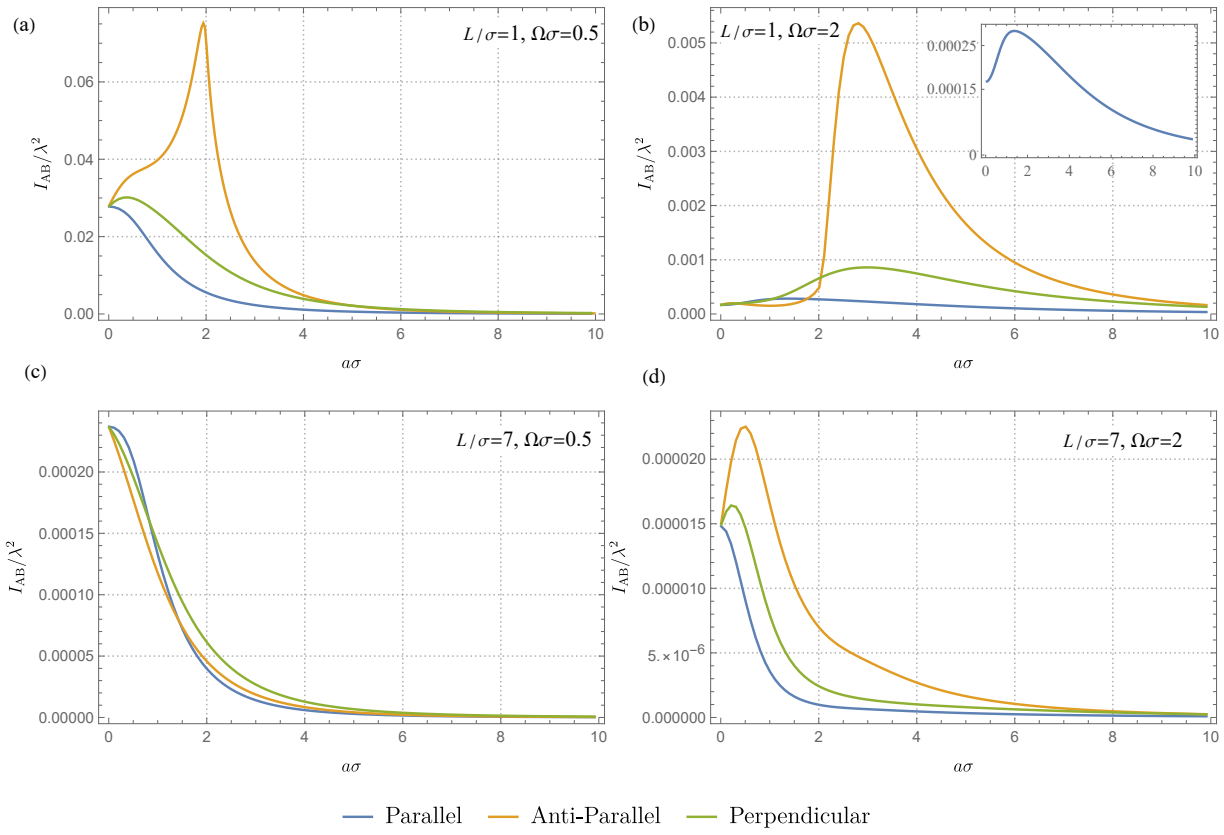

Figure 3.2: Mutual Information as a function of acceleration $a\sigma$ in three acceleration scenarios (parallel, anti-parallel, and perpendicular). (a) $L/\sigma = 1, \Omega\sigma = 0.5$, (b) $L/\sigma = 1, \Omega\sigma = 2$, (c) $L/\sigma = 7, \Omega\sigma = 0.5$, and (d) $L/\sigma = 7, \Omega\sigma = 2$.

discuss how different the temperature dependence among various scenarios is. Here, we focus on the difference between the accelerating detector scenarios and the thermal bath scenario in [42, 43].

Let us first review the thermal state of the scalar field. Let ρ_β be the KMS state of the scalar field. The corresponding Wightman function can be written as [43]

$$W_{\rm th}(\mathsf{x},\mathsf{x}') = W_{\rm M}(\mathsf{x},\mathsf{x}') + W_\beta(\mathsf{x},\mathsf{x}')\,, \tag{3.16}$$

where $W_{\rm M}(\mathsf{x},\mathsf{x}')$ is the Wightman function in the Minkowski vacuum given by (3.3) and $W_\beta(\mathsf{x},\mathsf{x}')$ is the contribution coming from the thermality, which reads (for a massless scalar

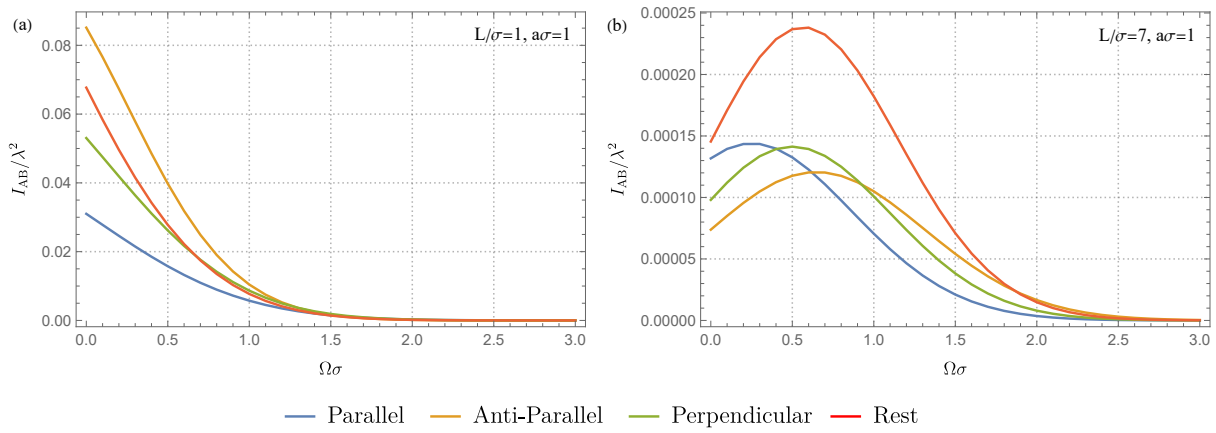

Figure 3.3: Mutual Information as a function of energy gap $\Omega\sigma$ in three acceleration scenarios (parallel, anti-parallel, and perpendicular) with $a\sigma = 1$ and (a) $L/\sigma = 1$, (b) $L/\sigma = 7$. The red curve represents the harvested mutual information by two inertial detectors in the Minkowski vacuum, which corresponds to $a\sigma = 0$.

field in $(3+1)$-dimensions)

$$W_\beta(\mathsf{x},\mathsf{x}') = \int \frac{\mathrm{d}^3k}{(2\pi)^3 2|\boldsymbol{k}|} \frac{e^{-\mathrm{i}|\boldsymbol{k}|(t-t')+\mathrm{i}\boldsymbol{k}\cdot(\boldsymbol{x}-\boldsymbol{x}')} + \text{c.c.}}{e^{\beta|\boldsymbol{k}|}-1}\,. \tag{3.17}$$

where $\beta \coloneqq T^{-1}$ is the inverse temperature.

From this Wightman function, one can calculate the elements in the density matrix. Let $\mathcal{M}^{\text{th}}$ and $\mathcal{L}^{\text{th}}_{ij}$ denote corresponding elements in the density matrix when the detectors are at rest in a thermal quantum field. Employing the concurrence

$$\mathcal{C}^{\text{th}}_{\text{AB}} \coloneqq 2\max\{0,\, |\mathcal{M}^{\text{th}}| - \sqrt{\mathcal{L}^{\text{th}}_{\text{AA}}\mathcal{L}^{\text{th}}_{\text{BB}}}\} \tag{3.18}$$

as a measure of entanglement, for temperatures satisfying $T_1 < T_2$, one can analytically show [43] that $\mathcal{C}^{\text{th}}_{\text{AB}}(T_1) > \mathcal{C}^{\text{th}}_{\text{AB}}(T_2)$, namely, the amount of entanglement between two inertial detectors in a thermal bath monotonically decreases with temperature. This is distinct from the case of uniformly accelerating detectors [55], where entanglement is either enhanced before vanishing at high temperature or monotonically decreases, depending on parameters such as the energy gap Ω. It is difficult to analytically show the behavior of quantum mutual information due to its logarithmic definition. However one can numerically check that the mutual information in a thermal bath monotonically increases

with temperature [43]. whereas our result (Fig. 3.2) shows similar behavior to that in the entanglement harvesting scenario with accelerating detectors [55].

Although an accelerating single detector experiences a thermal bath, two detectors exhibit remarkably different behavior. This can be explained by looking at their Wightman functions (3.16) and (3.7). One can examine this difference by, for example, performing a series expansion around $T = 0$:

$$W_{\rm th}(\mathsf{x},\mathsf{x}') = W_{\rm M}(\mathsf{x},\mathsf{x}') + \frac{T^2}{12} + \mathcal{O}(T^4)\,, \tag{3.19}$$

$$W_a(\mathsf{x},\mathsf{x}') = W_{\rm M}(\mathsf{x},\mathsf{x}') + c_1(\mathsf{x},\mathsf{x}')T_{\rm U} + c_2(\mathsf{x},\mathsf{x}')T_{\rm U}^2 + \mathcal{O}(T_{\rm U}^3)\,, \tag{3.20}$$

where the $c_j(\mathsf{x},\mathsf{x}')$ are expansion coefficients that depend on the spacetime points. Note that $W_{\rm th}(\mathsf{x},\mathsf{x}')$ has an expansion in even-powers of T for two arbitrary points x and x', and thereby along a single detector trajectory. On the other hand, for a single accelerating detector, these functions become $c_1(\mathsf{x},\mathsf{x}') = 0$ and $c_2(\mathsf{x},\mathsf{x}') = 1/12$, and so $W_a(\mathsf{x},\mathsf{x}')$ reduces to

$$W_a(\mathsf{x},\mathsf{x}') = W_{\rm M}(\mathsf{x},\mathsf{x}') + \frac{T_{\rm U}^2}{12} + \mathcal{O}(T_{\rm U}^4)\,, \tag{3.21}$$

which is equivalent to $W_{\rm th}(\mathsf{x},\mathsf{x}')$. Apparently, the Wightman functions along two trajectories differ, whereas the ones on a single trajectory match. It is not so surprising that two distinct Wightman functions give different correlations. If we specify the state of the field and the trajectories of the detectors in such a way that two Wightman functions match, the corresponding quantities such as concurrence or transition probability behave in the same way, which is the case for a single accelerating detector.

As an application of this observation, consider two UDW detectors in an expanding universe considered in [41, 71]. The line element of the de Sitter spacetime in the planar coordinates is

$$\mathrm{d}s^2 = -\mathrm{d}t^2 + e^{2\kappa t}(\mathrm{d}x^2 + \mathrm{d}y^2 + \mathrm{d}z^2)\,, \tag{3.22}$$

where κ is the expansion rate of the universe. We employ a conformally coupled, massless scalar field in the conformal vacuum. In this case, a single inertial detector also sees a thermal bath at temperature $T_{\rm GH} \coloneqq \kappa/2\pi$ (the Gibbons-Hawking effect [72]). This can be seen from the Wightman function [61],

$$W_{\rm dS}(\mathsf{x},\mathsf{x}') = -\frac{1}{4\pi^2}\frac{1}{\dfrac{\sinh^2(\pi T_{\rm GH}\Delta t - \mathrm{i}\epsilon)}{\pi^2 T_{\rm GH}^2} - e^{2\pi T_{\rm GH}\Delta_+ t}L^2}\,, \tag{3.23}$$

$$(\Delta t \equiv t - t',\ \Delta_+ t \equiv t + t')\,,$$

by pulling it back to a single inertial trajectory, $L = 0$, which yields the same form as (3.6). Nevertheless, in the case of $L \neq 0$, a series expansion of $W_{\rm dS}(\mathsf{x}, \mathsf{x}')$ around $T_{\rm GH} = 0$ reads

$$W_{\rm dS}(\mathsf{x}, \mathsf{x}') = W_{\rm M}(\mathsf{x}, \mathsf{x}') + c_1^{\rm dS}(\mathsf{x}, \mathsf{x}')T_{\rm GH} + c_2^{\rm dS}(\mathsf{x}, \mathsf{x}')T_{\rm GH}^2 + \mathcal{O}(T_{\rm GH}^3)\,, \tag{3.24}$$

where c_i^{dS} with $i \in \{1, 2, ...\}$ are non-zero coefficients. The explicit expressions are rather complicated functions of L and t, and are not needed for our purposes so we will not delve into them.
We can see obviously that $W_{\rm dS}(\mathsf{x}, \mathsf{x}')$ differs from $W_{\rm th}(\mathsf{x}, \mathsf{x}')$ in (3.19).
In summary, harvested correlations do not necessarily show the same behavior even if two scenarios give the same transition probability. This is simply because the Wightman functions are different in general between distinct spacetime points on different trajectories. These quantities, including transition probability, show identical features if the Wightman functions in two scenarios happen to be the same.

3.2 Summary

We have investigated the harvesting protocol for mutual information with two uniformly accelerating detectors in the Minkowski vacuum. Our main purpose was to fill in the missing piece of the correlation harvesting protocol for situations in which a single detector perceives a thermal bath. These include a uniformly accelerating detector, a static detector in a black hole spacetime, and an inertial detector in de Sitter spacetime.

As with the entanglement harvesting scenario revisited recently [55], we considered three types of acceleration scenarios: parallel, anti-parallel, and perpendicular. We found that, as for the entanglement harvesting case, acceleration can enhance mutual information for certain detector separations and energy gaps. Moreover, it asymptotically vanishes as the acceleration (equivalently, the Unruh temperature) increases. This is in contrast to the case of two inertial detectors in a thermal bath [42, 43], where mutual information monotonically increases with the bath temperature. We have also looked into the energy gap dependence and found that there is a range of energy gaps in which either classical correlations or nondistillable entanglement can be extracted from the field.

Our analysis provides a complete picture of correlation harvesting with thermalized detectors. The take-home lesson is that the temperature dependence of harvested correlations differs among different scenarios even when a single detector responds in the same manner for each. This is not surprising since the properties of harvested correlations depend on the Wightman function (a two-point correlation function of a quantum

field) $W(\mathsf{x},\mathsf{y}) = \mathrm{Tr}[\rho_\phi \hat{\phi}(\mathsf{x})\hat{\phi}(\mathsf{y})]$, where ρ_ϕ is the state of the field $\hat{\phi}$, which is in general different among different systems. Given the state of the field ρ_ϕ and the trajectories of detectors, if the functional forms of the Wightman function are different, then one should expect different results for correlation harvesting. Nevertheless, if the functional forms of $W(\mathsf{x},\mathsf{y})$ happen to be identical, then the harvested correlations would show the same behavior. In the case of inertial detectors in a thermal bath in [43] and our uniformly accelerating detectors in the Minkowski vacuum, their Wightman functions are different, and so the temperature dependence of entanglement as well as mutual information differs. However, if we look at a single detector, the functional forms of the Wightman functions along this trajectory are identical, which is the reason that a single detector undergoing uniform acceleration experiences thermality as if it is immersed in a thermal bath at temperature $T_{\mathrm{U}} = a/2\pi$. Beyond the mathematical framework, one may also inquire into the physical reason underlying the difference in temperature-dependent correlation behavior between inertial and non-inertial systems. A plausible explanation could be the influence of the relativistic Doppler shift, which is mediated by time dilation effects. However, this necessitates further research and investigation for validation.

Chapter 4

Correlation harvesting between particle detectors in uniform motion

In this chapter, we extend our study to investigate the correlation harvesting protocol using two Unruh-DeWitt particle detectors moving along four classes of uniformly accelerated trajectories categorized by Letaw[3]: linear, catenary, cusped, and circular motions. For each trajectory, two types of configurations are carried out: one possesses a stationary (time-translation invariant) Wightman function and the other is nonstationary. We find that detectors undergoing linear, catenary, and cusped motions gain fewer correlations in the nonstationary configurations compared to those in stationary configurations. Detectors in circular motion have similar behavior in both configurations. We discuss the relative suppression of correlation harvesting due to high acceleration for each case. Remarkably we find that under certain circumstances detectors in both linear and circular states of motion can harvest genuine (non-communication assisted) entanglement even though they are in causal contact.

This study is motivated by the ongoing experiments aimed at verifying the Unruh effect. A primary obstacle in the verification of Unruh temperature lies in the immense acceleration needed to generate experimentally measurable temperatures. For instance, an acceleration on the order of magnitude $a \approx 10^{20}\,\mathrm{m/s^2}$ is required to achieve a temperature of $T_{\mathrm{U}} \sim 1$ Kelvin. This considerable requirement motivates the exploration of alternative trajectories that can more easily be implemented in laboratory settings yet still induce phenomena analogous to the Unruh effect.

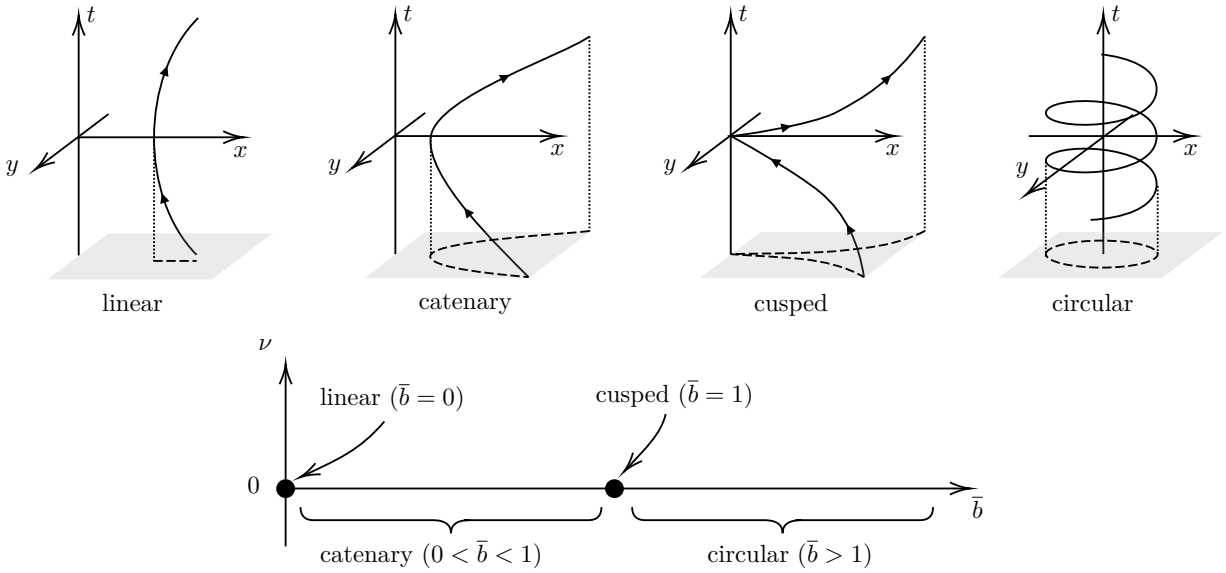

Figure 4.1: Four trajectories characterized by $\bar{b} \equiv b/a$.

4.1 Uniform acceleration trajectories

4.1.1 Single detector trajectory classification

The most well-known trajectory for a uniformly accelerating (i.e., $a = const.$) pointlike particle is linear accelerated motion that we discussed in last chapter. However, Letaw pointed out that there are, in fact, five classes of uniformly accelerated trajectories, excluding the case where $a = 0$. Along with the linear case, the other classes are circular, catenary, cusped, and helix. Consider a trajectory in $(3+1)$-dimensional Minkowski spacetime. Such a trajectory can be characterized by three geometric invariants: the curvature $a(\tau)$, which represents the magnitude of proper acceleration, the first torsion $b(\tau)$, and the second torsion (also known as hypertorsion) $\nu(\tau)$ of the worldline. The torsions $b(\tau)$ and $\nu(\tau)$ correspond to the proper angular velocities in a given tetrad frame [3]. Assuming that these invariants are constants, the trajectory becomes stationary. In a nutshell, these motions are characterized by the following:

1. linear: $a \neq 0, b = \nu = 0$
2. catenary: $a > b$, $\nu = 0$

3. cusped: $a = b, \nu = 0$
4. circular: $a < b, \nu = 0$
5. helix: $\nu \neq 0$

In this subsection, we review these trajectories and consider the corresponding vacuum Wightman functions. We will suppress the UV cutoff ϵ for readability.

Linear motion

The linear acceleration motion of a detector is defined solely by the constant acceleration a, with all other parameters set to zero. The trajectory reads

$$\mathsf{x}(\tau) = \left(\frac{1}{a}\sinh(a\tau), \frac{1}{a}\cosh(a\tau), 0, 0\right) , \tag{4.1}$$

and the Wightman function along this trajectory is given by

$$W_{\text{lin}}(\Delta\tau) = -\frac{1}{4\pi^2}\frac{1}{\frac{4}{a^2}\sinh^2\left(\frac{a\Delta\tau}{2}\right)} , \tag{4.2}$$

where $\Delta\tau \coloneqq \tau - \tau'$.

Circular motion

The circular trajectory is defined by a and b satisfying $a < b$. Let us begin with a commonly used trajectory

$$\mathsf{x}(\tau) = (\gamma\tau, R\cos(\omega\gamma\tau), R\sin(\omega\gamma\tau), 0) , \tag{4.3}$$

where R, ω, and γ are the radius of the circular motion, angular velocity, and the Lorentz factor defined as $\gamma \coloneqq 1/\sqrt{1-v^2}$. Here, $v \coloneqq R\omega(\leq 1)$ is the speed of the detector. Introducing the acceleration of the detector $a = R\omega^2\gamma^2$, these parameters can be related by

$$\omega = \sqrt{\frac{a}{(1+aR)R}} , \tag{4.4a}$$

$$\gamma = \sqrt{1+aR} , \tag{4.4b}$$

$$v = \sqrt{\frac{aR}{1+aR}} . \tag{4.4c}$$

In terms of the acceleration a and the torsion b, we can further express ω and v as

$$\omega = b(1 - a^2/b^2) \qquad v = a/b$$

respectively. The Wightman function is then

$$W_{\rm cir}(\Delta\tau) = -\frac{1}{4\pi^2}\frac{1}{\gamma^2\Delta\tau^2 - 4R^2\sin^2(\omega\gamma\Delta\tau/2)}\,. \tag{4.5}$$

Cusped motion

Cusped motion is described by the acceleration and torsion with $a = b$. The trajectory reads

$$\mathsf{x}(\tau) = \left(\tau + \frac{1}{6}a^2\tau^3,\, \frac{1}{2}a\tau^2,\, \frac{1}{6}a^2\tau^3,\, 0\right)\,, \tag{4.6}$$

and the corresponding Wightman function is

$$W_{\rm cus}(\Delta\tau) = -\frac{1}{4\pi^2}\frac{1}{\Delta\tau^2 + \dfrac{a^2}{12}\Delta\tau^4}\,. \tag{4.7}$$

Catenary motion

Catenary motion can be characterized by a and b with $a > b$. The trajectory is given by

$$\mathsf{x}(\tau) = \left(\frac{a}{a^2-b^2}\sinh\left(\sqrt{a^2-b^2}\,\tau\right), \frac{a}{a^2-b^2}\cosh\left(\sqrt{a^2-b^2}\,\tau\right), \frac{b\tau}{\sqrt{a^2-b^2}}, 0\right)\,, \tag{4.8}$$

and the Wightman function reads

$$W_{\rm cat}(\Delta\tau) = -\frac{1}{4\pi^2}\frac{1}{-\dfrac{b^2\Delta\tau^2}{a^2-b^2} + \dfrac{4a^2}{(a^2-b^2)^2}\sinh^2\left(\frac{\sqrt{a^2-b^2}\Delta\tau}{2}\right)}. \tag{4.9}$$

We immediately see that catenary motion reduces to linear motion as $b \to 0$. Catenary motion also reduces to cusped motion as $b \to a$ after a coordinate transformation consisting of a Lorentz boost a translation [73].

Helix motion

Finally, helix motion is a combination of circular and linear acceleration motions characterized by three parameters, a, b, and ν:

$$\mathsf{x}(\tau) = \left(\frac{\mathcal{P}}{\Gamma_+} \sinh(\Gamma_+\tau), \frac{\mathcal{P}}{\Gamma_+} \cosh(\Gamma_+\tau), \right. \\ \left. \frac{\mathcal{Q}}{\Gamma_-} \cos(\Gamma_-\tau), \frac{\mathcal{Q}}{\Gamma_-} \sin(\Gamma_-\tau) \right), \tag{4.10}$$

where $\mathcal{P} \coloneqq \Xi/\Gamma$, $\mathcal{Q} \coloneqq ab/\Xi\Gamma$, and

$$\Xi^2 \coloneqq \frac{1}{2}(\Gamma^2 + a^2 + b^2 + \nu^2)\,, \tag{4.11a}$$

$$\Gamma^2 \coloneqq \Gamma_+^2 + \Gamma_-^2\,, \quad \Gamma_\pm^2 \coloneqq \sqrt{A^2 + B^2} \pm A\,, \tag{4.11b}$$

$$A \coloneqq \frac{1}{2}(a^2 - b^2 - \nu^2)\,, \quad B \coloneqq a\nu\,. \tag{4.11c}$$

The Wightman function reads

$$W_{\text{hel}}(\Delta\tau) = -\frac{1}{4\pi^2} \frac{1}{\frac{4\mathcal{P}^2}{\Gamma_+^2} \sinh^2\left(\frac{\Gamma_+\Delta\tau}{2}\right) - \frac{4\mathcal{Q}^2}{\Gamma_-^2} \sin^2\left(\frac{\Gamma_-\Delta\tau}{2}\right)}\,. \tag{4.12}$$

Note that the trajectory and the corresponding Wightman function reduce to the aforementioned trajectories when $\nu \to 0$. In this sense, the helix is the general motion that contains other motions.

Wightman function at $\nu = 0$

We now turn our attention to the special case where $\nu = 0$. Although the Wightman functions for linear, circular, catenary, and cusped motions may initially appear to take different forms, they can actually be expressed in a unified manner. Let $\bar{b} \equiv b/a$ with the condition that $a \neq 0$. The Wightman functions for all trajectories with $\nu = 0$ can be written in the following compact form:

$$W_{\nu=0}(\Delta\tau) = -\frac{1}{4\pi^2} \frac{1}{-\frac{\bar{b}^2}{1-\bar{b}^2}\Delta\tau^2 + \frac{4}{(1-\bar{b}^2)^2 a^2} \sinh^2\left(\frac{\sqrt{1-\bar{b}^2}a\Delta\tau}{2}\right)}\,. \tag{4.13}$$

The parameter $\bar{b}$ serves to specify the particular trajectory, as illustrated in figure 4.1: linear ($\bar{b} = 0$), catenary ($0 < \bar{b} < 1$), cusped ($\bar{b} = 1$), and circular ($\bar{b} > 1$). For circular motion, we employ the identity $\sin(\mathrm{i}x) = \mathrm{i}\sinh(x)$. Note that one obtains the Wightman function for the cusped motion, as given in (4.7), by performing a series expansion around $\bar{b} = 1$.

The corresponding transition probability $\mathcal{L}_{jj}$, $j \in \{\mathrm{A}, \mathrm{B}\}$, in (2.31) reads

$$\mathcal{L}_{jj} = \lambda^2 \sigma \sqrt{\pi} \int_{\mathbb{R}} \mathrm{d}u \, e^{-u^2/4\sigma^2} e^{-\mathrm{i}\Omega u} W_{\nu=0}(u) \,. \tag{4.14}$$

4.1.2 Two detectors in uniform acceleration

We now consider two UDW detectors A and B, both undergoing uniform acceleration motion. In particular, we categorize the detector configurations into two classes: stationary (time-translation invariant) and nonstationary scenarios.

Stationary scenario

Consider two detectors undergoing the same uniform acceleration (e.g., both linearly accelerated). The Wightman function can be made time-translation invariant, meaning it depends only on the time difference $\Delta\tau \coloneqq \tau_{\mathrm{A}} - \tau_{\mathrm{B}}$, by imposing that the angle between the velocity vector of a detector and the spatial displacement vector from one detector to the other is time-independent. For example, two linearly accelerating detectors along the trajectories

$$\mathsf{x}_{\mathrm{A}}(\tau_{\mathrm{A}}) = \left(\frac{1}{a}\sinh(a\tau_{\mathrm{A}}), \frac{1}{a}\cosh(a\tau_{\mathrm{A}}), 0, 0\right) , \tag{4.15a}$$

$$\mathsf{x}_{\mathrm{B}}(\tau_{\mathrm{B}}) = \left(\frac{1}{a}\sinh(a\tau_{\mathrm{B}}), \frac{1}{a}\cosh(a\tau_{\mathrm{B}}), L, 0\right) \tag{4.15b}$$

give the following stationary Wightman function:

$$W_{\mathrm{lin}}(\tau_{\mathrm{A}}, \tau_{\mathrm{B}}) = -\frac{1}{4\pi^2} \frac{1}{\frac{4}{a^2}\sinh^2\left(\frac{a\Delta\tau}{2}\right) - L^2} \tag{4.16}$$

where $L \coloneqq |\boldsymbol{x}_{\mathrm{A}} - \boldsymbol{x}_{\mathrm{B}}|$ is the spatial separation between the two detectors. As depicted in figure 4.2 top-left, each velocity vector of the detector is always perpendicular to the displacement vector $\boldsymbol{x}_{\mathrm{AB}} \coloneqq \boldsymbol{x}_{\mathrm{A}} - \boldsymbol{x}_{\mathrm{B}}$ throughout the interaction.

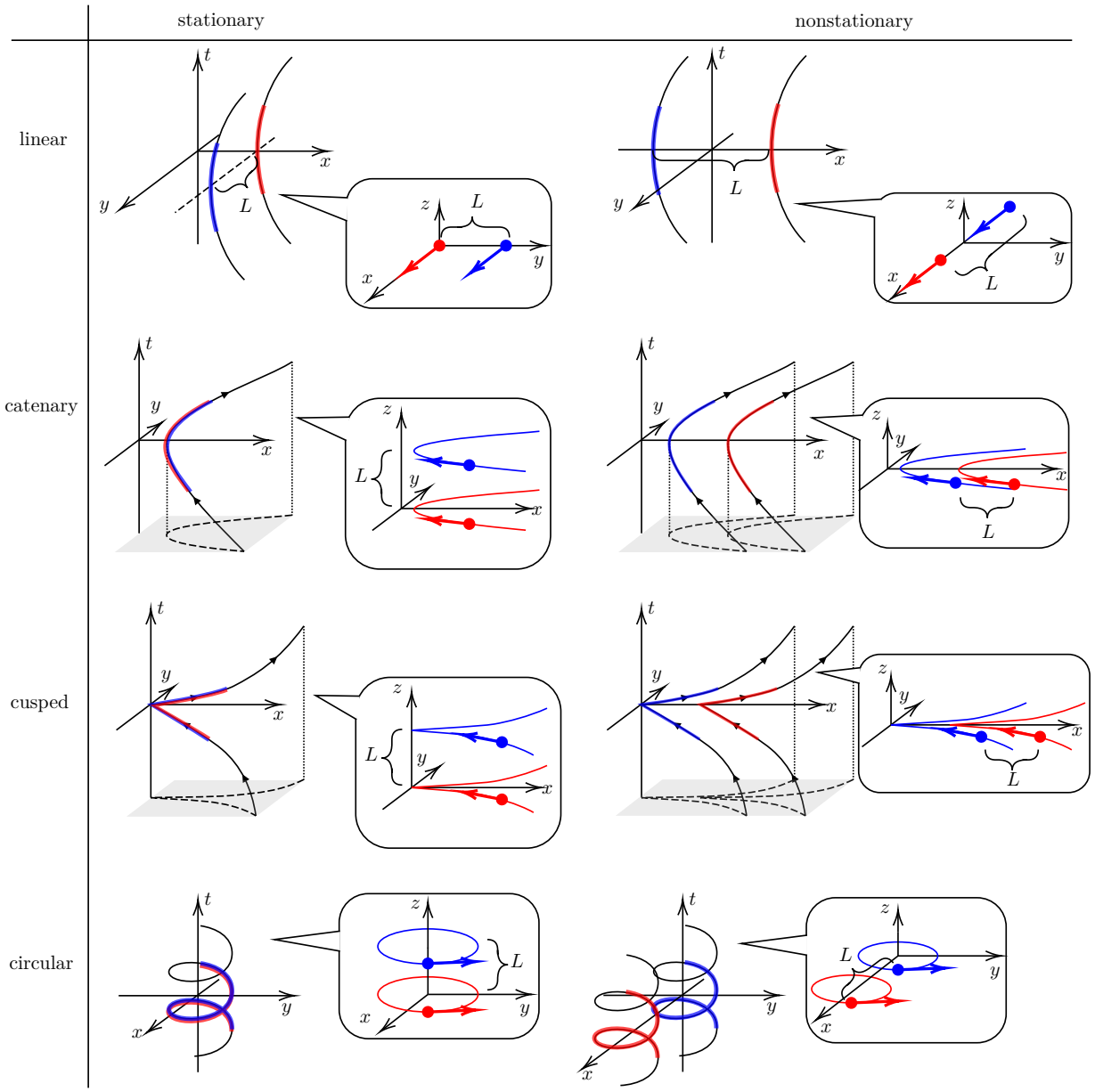

Figure 4.2: Stationary and nonstationary configurations for four classes of uniformly accelerating detectors. Red and blue strips represent detectors A and B, respectively.

We can also construct stationary Wightman functions for other motions:

circular:

$$\mathsf{x}_{\mathrm{A}} = (\gamma\tau_{\mathrm{A}}, R\cos(\omega\gamma\tau_{\mathrm{A}}), R\sin(\omega\gamma\tau_{\mathrm{A}}), 0)\ , \tag{4.17a}$$
$$\mathsf{x}_{\mathrm{B}} = (\gamma\tau_{\mathrm{B}}, R\cos(\omega\gamma\tau_{\mathrm{B}}), R\sin(\omega\gamma\tau_{\mathrm{B}}), L)\ . \tag{4.17b}$$

cusped:

$$\mathsf{x}_{\mathrm{A}} = \left(\tau_{\mathrm{A}} + \frac{1}{6}a^2\tau_{\mathrm{A}}^3,\ \frac{1}{2}a\tau_{\mathrm{A}}^2,\ \frac{1}{6}a^2\tau_{\mathrm{A}}^3,\ 0\right)\ , \tag{4.18a}$$
$$\mathsf{x}_{\mathrm{B}} = \left(\tau_{\mathrm{B}} + \frac{1}{6}a^2\tau_{\mathrm{B}}^3,\ \frac{1}{2}a\tau_{\mathrm{B}}^2,\ \frac{1}{6}a^2\tau_{\mathrm{B}}^3,\ L\right)\ , \tag{4.18b}$$

catenary:

$$\mathsf{x}_{\mathrm{A}} = \left(\frac{a}{a^2-b^2}\sinh\left(\sqrt{a^2-b^2}\,\tau_{\mathrm{A}}\right), \frac{a}{a^2-b^2}\cosh\left(\sqrt{a^2-b^2}\,\tau_{\mathrm{A}}\right), \frac{b\tau_{\mathrm{A}}}{\sqrt{a^2-b^2}}, 0\right)\ , \tag{4.19a}$$
$$\mathsf{x}_{\mathrm{B}} = \left(\frac{a}{a^2-b^2}\sinh\left(\sqrt{a^2-b^2}\,\tau_{\mathrm{B}}\right), \frac{a}{a^2-b^2}\cosh\left(\sqrt{a^2-b^2}\,\tau_{\mathrm{B}}\right), \frac{b\tau_{\mathrm{B}}}{\sqrt{a^2-b^2}}, L\right)\ , \tag{4.19b}$$

As for a single detector, the Wightman functions along the trajectories given above take the following compact form:

$$W_{\mathrm{s}}(\tau_{\mathrm{A}},\tau_{\mathrm{B}}) \equiv W_{\mathrm{s}}(\Delta\tau) = -\frac{1}{4\pi^2}\frac{1}{-\dfrac{\bar{b}^2}{1-\bar{b}^2}\Delta\tau^2 + \dfrac{4}{(1-\bar{b}^2)^2a^2}\sinh^2\left(\dfrac{\sqrt{1-\bar{b}^2}a\Delta\tau}{2}\right) - L^2}\ , \tag{4.20}$$

where $\Delta\tau \coloneqq \tau_{\mathrm{A}} - \tau_{\mathrm{B}}, \bar{b} \equiv b/a$, and the subscript 's' stands for stationary. Since the Wightman function depends only on $\Delta\tau$, the elements in the density matrix (2.31), $\mathcal{M}$ and $\mathcal{L}_{\mathrm{AB}}$, can be simplified to single integrals when the Gaussian switching function (2.38) is used:

$$\mathcal{M} = -2\lambda^2\sigma\sqrt{\pi}e^{-\Omega^2\sigma^2}\int_0^\infty \mathrm{d}u\, e^{-u^2/4\sigma^2}W_{\mathrm{s}}(u)\,, \tag{4.21a}$$
$$\mathcal{L}_{\mathrm{AB}} = \lambda^2\sigma\sqrt{\pi}\int_{\mathbb{R}} \mathrm{d}u\, e^{-u^2/4\sigma^2}e^{-\mathrm{i}\Omega u}W_{\mathrm{s}}(u)\,. \tag{4.21b}$$

Here, we used the fact that the Heaviside step function in (2.32b) can be written as $\Theta(t(\tau_{\mathrm{A}}) - t(\tau_{\mathrm{B}})) = \Theta(\tau_{\mathrm{A}} - \tau_{\mathrm{B}})$ for any of the uniform acceleration scenarios mentioned earlier.

We note that all stationary configurations can only be realized in $(3+1)$ dimensions, with the exception of the linear configuration.

Nonstationary scenario

One can also consider configurations similar to those in section 4.1.2, where the Wightman function depends not only on $\Delta\tau$ but also on $\Delta_+\tau \coloneqq \tau_\mathrm{A} + \tau_\mathrm{B}$. In this case, the Wightman function is no longer time-translation invariant (hence, nonstationary).

In particular, consider two linearly accelerating UDW detectors whose trajectories are given by

$$\mathsf{x}_\mathrm{A}(\tau_\mathrm{A}) = \left(\frac{1}{a}\sinh(a\tau_\mathrm{A}), \frac{1}{a}\cosh(a\tau_\mathrm{A}) + L, 0, 0\right) , \tag{4.22a}$$

$$\mathsf{x}_\mathrm{B}(\tau_\mathrm{B}) = \left(\frac{1}{a}\sinh(a\tau_\mathrm{B}), \frac{1}{a}\cosh(a\tau_\mathrm{B}), 0, 0\right) . \tag{4.22b}$$

The correlation harvesting protocol along these trajectories was examined in [55, 59] and discussed in last chapter. The corresponding Wightman function reads

$$W_\mathrm{lin}(\tau_\mathrm{A}, \tau_\mathrm{B}) = -\frac{1}{4\pi^2}\frac{1}{\frac{4}{a^2}\sinh^2\left(\frac{a\Delta\tau}{2}\right) - L^2 - \frac{4L}{a}\sinh\left(\frac{a\Delta\tau}{2}\right)\sinh\left(\frac{a\Delta_+\tau}{2}\right)} . \tag{4.23}$$

The term $\Delta_+\tau$ comes from the fact that the angle between the velocity vector and the displacement vector is time-dependent (0° or 180°).

Similarly, other uniformly accelerating trajectories that yield a nonstationary Wightman function are

circular:

$$\mathsf{x}_\mathrm{A} = (\gamma\tau_\mathrm{A}, R\cos(\omega\gamma\tau_\mathrm{A}) + L, R\sin(\omega\gamma\tau_\mathrm{A}), 0) , \tag{4.24a}$$

$$\mathsf{x}_\mathrm{B} = (\gamma\tau_\mathrm{B}, R\cos(\omega\gamma\tau_\mathrm{B}), R\sin(\omega\gamma\tau_\mathrm{B}), 0) . \tag{4.24b}$$

cusped:

$$\mathsf{x}_\mathrm{A} = \left(\tau_\mathrm{A} + \frac{1}{6}a^2\tau_\mathrm{A}^3, \frac{1}{2}a\tau_\mathrm{A}^2 + L, \frac{1}{6}a^2\tau_\mathrm{A}^3, 0\right) , \tag{4.25a}$$

$$\mathsf{x}_\mathrm{B} = \left(\tau_\mathrm{B} + \frac{1}{6}a^2\tau_\mathrm{B}^3, \frac{1}{2}a\tau_\mathrm{B}^2, \frac{1}{6}a^2\tau_\mathrm{B}^3, 0\right) , \tag{4.25b}$$

catenary:

$$\mathsf{x}_\mathrm{A} = \left(\frac{a}{a^2-b^2}\sinh\left(\sqrt{a^2-b^2}\,\tau_\mathrm{A}\right), \frac{a}{a^2-b^2}\cosh\left(\sqrt{a^2-b^2}\,\tau_\mathrm{A}\right) + L, \frac{b\tau_\mathrm{A}}{\sqrt{a^2-b^2}}, 0\right) , \tag{4.26a}$$

$$\mathsf{x}_\mathrm{B} = \left(\frac{a}{a^2-b^2}\sinh\left(\sqrt{a^2-b^2}\,\tau_\mathrm{B}\right), \frac{a}{a^2-b^2}\cosh\left(\sqrt{a^2-b^2}\,\tau_\mathrm{B}\right), \frac{b\tau_\mathrm{B}}{\sqrt{a^2-b^2}}, 0\right) , \tag{4.26b}$$

The Wightman function for these nonstationary motions can be compactly expressed as

$$W_{\rm ns}(\tau_{\rm A},\tau_{\rm B}) = -\frac{1}{4\pi^2}\frac{1}{-\frac{\bar{b}^2}{1-\bar{b}^2}\Delta\tau^2+\frac{4}{(1-\bar{b}^2)^2a^2}\sinh^2\left(\frac{\sqrt{1-\bar{b}^2}a\Delta\tau}{2}\right)-L^2-\frac{4L}{(1-\bar{b}^2)a}\sinh\left(\frac{\sqrt{1-\bar{b}^2}a\Delta\tau}{2}\right)\sinh\left(\frac{\sqrt{1-\bar{b}^2}a\Delta_+\tau}{2}\right)} \tag{4.27}$$

and possesses an additional term in the denominator compared to the stationary Wightman function (4.20). Here, the subscript 'ns' designates nonstationary. Due to this additional term, the correlations harvested by nonstationary detectors will exhibit behavior similar to those of stationary detectors.

Note that the presence of $\Delta_+\tau$ prevents us from reducing the double integrals in (2.32) into single integrals. Furthermore, all nonstationary configurations can be realized in (2+1) dimensions, except for the helix case, which we are not considering.

4.2 Numerical results

Here, we numerically compute the concurrence (2.35) and quantum mutual information (2.36) harvested by two uniformly accelerating detectors by inserting the Wightman functions (4.13), (4.20) and (4.27) into $\mathcal{L}_{ij}$ and $\mathcal{M}$ given in (2.32). For stationary detectors in 4.1.2, we utilize the expressions given by (4.21).

4.2.1 Transition probability of uniformly accelerating detectors

Let us begin by considering the transition probability $\mathcal{L}_{jj}$ for a uniformly accelerating detector. We are particularly interested in the cases of linear ($\bar{b}=0$), catenary ($0<\bar{b}<1$), cusped ($\bar{b}=1$), and circular ($\bar{b}>1$) motions, and their respective transition probabilities are given by (4.14). We consider $\mathcal{L}_{jj}/\lambda^2$ and write the parameters in units of σ, which makes the transition probability a function of three variables: $a\sigma, \bar{b}$, and $\Omega\sigma$. It is important to note that $\mathcal{L}_{\rm AA}=\mathcal{L}_{\rm BB}$, as we are assuming both detectors are identical.

Figure 4.3 depicts the transition probability $\mathcal{L}_{jj}/\lambda^2$ as a function of the magnitude of acceleration $a\sigma$ for fixed Ω (panel (a)) and $\log_{10}\bar{b}$ for different values of the acceleration (panels (b), (c)). In figure 4.3(a), the transition probabilities for a detector with $\Omega\sigma=2$ in

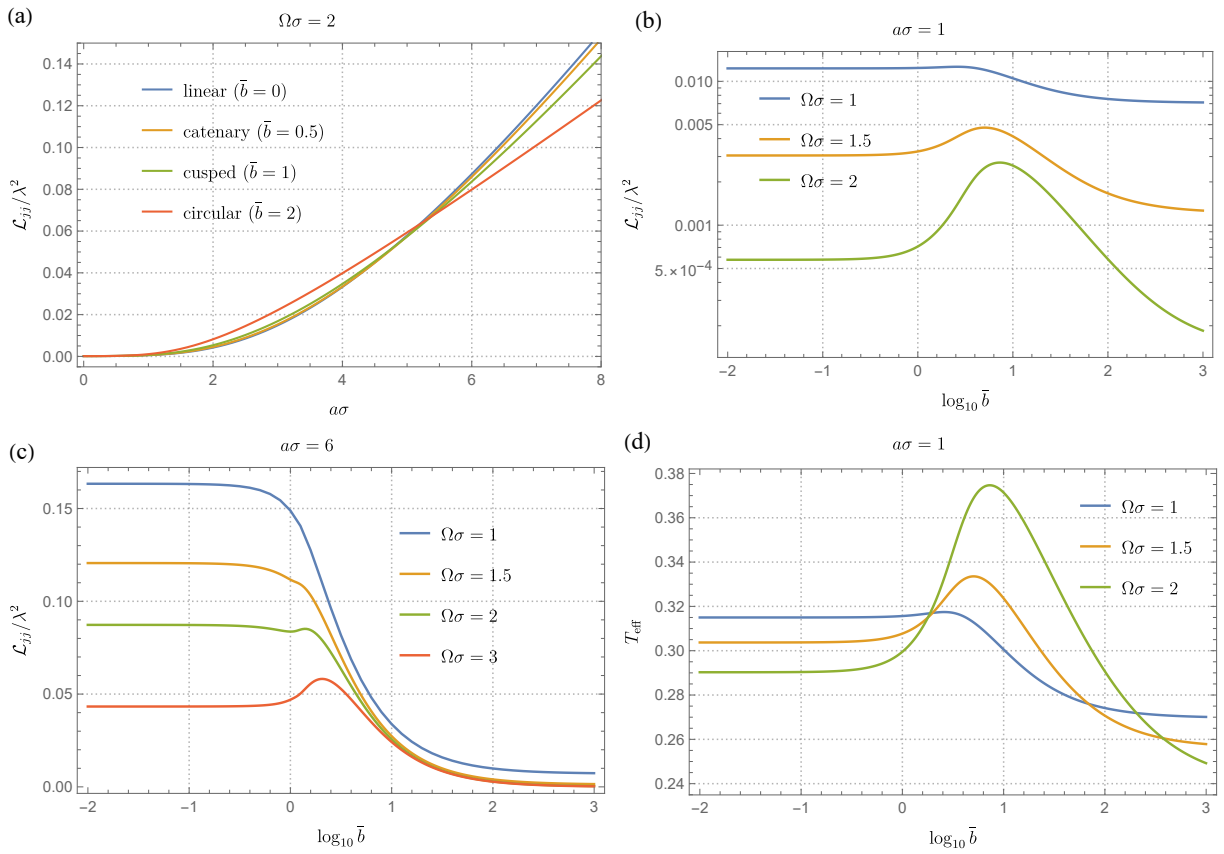

Figure 4.3: (a) Transition probabilities $\mathcal{L}_{jj}/\lambda^2$ as a function of the magnitude of acceleration $a\sigma$ with $\Omega\sigma = 2$. (b) $\mathcal{L}_{jj}/\lambda^2$ as a function of $\log_{10}\bar{b}$ with $a\sigma = 1$ and (c) with $a\sigma = 6$. (d) The effective temperature T_{eff} as a function of $\log_{10}\bar{b}$ with $a\sigma = 1$.

linear ($\bar{b} = 0$), catenary ($\bar{b} = 0.5$), cusped ($\bar{b} = 1$), and circular ($\bar{b} = 2$) motions are shown. We find that in all these cases, $\mathcal{L}_{jj}/\lambda^2$ increases with the acceleration $a\sigma$.[1]

However, the relationship between the transition probabilities of detectors in different uniform motions is highly nontrivial. For instance, when a detector has $\Omega\sigma = 2$ and $a\sigma \lesssim 5$, as depicted in figure 4.3(a), a detector in circular motion with $\bar{b} = 2$ shows the largest value of $\mathcal{L}_{jj}/\lambda^2$, whereas a detector in linear motion ($\bar{b} = 0$) shows the smallest. This relation,

[1] $\mathcal{L}_{jj}/\lambda^2$ is not guaranteed to *monotonically* increase with $a\sigma$ for a finite interaction duration. For a detector in the linearly accelerated motion, such a phenomenon is known as the (weak) anti-Unruh effect [74, 75].

however, flips for $a\sigma \gtrsim 5$. We will numerically demonstrate that such relationships depend on the interplay between $a\sigma$ and $\Omega\sigma$.

In figure 4.3(b), the magnitude of the acceleration is fixed at $a\sigma = 1$, and $\mathcal{L}_{jj}/\lambda^2$ is plotted as a function of $\log_{10}\bar{b}$. Each curve in this figure corresponds to a different value of $\Omega\sigma$, with the curve for $\Omega\sigma = 2$ corresponding to figure 4.3(a) at $a\sigma = 1$. For each value of $\Omega\sigma$ in 4.3(b), the transition probability has a peak for $\log_{10}\bar{b} > 0$ (i.e., $\bar{b} > 1$), and then decreases with increasing $\log_{10}\bar{b}$, becoming smaller than the value for the linear case ($\log_{10}\bar{b} \to -\infty$). This means that $\mathcal{L}_{jj}/\lambda^2$ at $a\sigma = 1$ in figure 4.3(a) increases with $\bar{b}$ until it reaches a maximum and then decreases. We note that the presence of the peak is contingent on larger values of $\Omega\sigma$ relative to $a\sigma$; In fact, the peak does not appear for smaller energy gaps, in which case the transition probability monotonically decreases with $\bar{b}$, as shown in figure 4.3(b). This trend is further illustrated in figure 4.3(c), where $a\sigma = 6$ is chosen. In this scenario, the peak is nonexistent for $\Omega\sigma = 1$ and 1.5 (as well as for $\Omega\sigma < 1$), but becomes manifest when $\Omega\sigma \gtrsim 2$. Thus we infer that detectors with smaller energy gaps $\Omega\sigma$ compared to $a\sigma$ do not have a peak in $\mathcal{L}_{jj}(\bar{b})/\lambda^2$.

The behavior of $\mathcal{L}_{jj}/\lambda^2$ is related to the concept of the "effective temperature" perceived by a detector. For now, let us denote the transition probability as $\mathcal{L}_{jj}(\Omega, \sigma)$. The effective temperature, T_{eff}, is defined as

$$T_{\text{eff}}^{-1} \coloneqq \frac{1}{\Omega} \ln \frac{\mathcal{L}_{jj}(-\Omega, \sigma)/\lambda^2\sigma}{\mathcal{L}_{jj}(\Omega, \sigma)/\lambda^2\sigma} \tag{4.28}$$

where this formula is derived in the Appendix. We divide $\mathcal{L}_{jj}(\Omega, \sigma)$ by σ so that it is well defined in the long interaction limit, $\sigma \to \infty$ [76, 75]. Note that if the Wightman function obeys the Kubo-Martin-Schwinger (KMS) condition [62, 63], then the effective temperature converges to the KMS temperature (which is the temperature of the field formally defined in quantum field theory) in the limit $\sigma \to \infty$. However, in the case of finite interaction duration, the effective temperature is an estimator for the actual field temperature. For a detector in a uniform acceleration motion, the effective temperature for each scenario has been examined in, e.g., [77, 78, 79, 80, 73, 8, 7].

We plot the effective temperature T_{eff} as a function of $\log_{10}\bar{b}$ when $\sigma = 1$ and $a\sigma = 1$ in figure 4.3(d), which corresponds to figure 4.3(b). We see that the locations of the peaks in T_{eff} align with those of $\mathcal{L}_{jj}(\Omega)$ in 4.3(b). This suggests that, for a given acceleration and energy gap, a detector in circular motion within a certain range of $\log_{10}\bar{b}$ can register higher effective temperatures than those in other types of motion. However, as $\bar{b} \to \infty$, which corresponds to the speed of a detector in circular motion with $v_{\text{circ}}(= \bar{b}^{-1}) \to 0$, the temperature becomes colder.

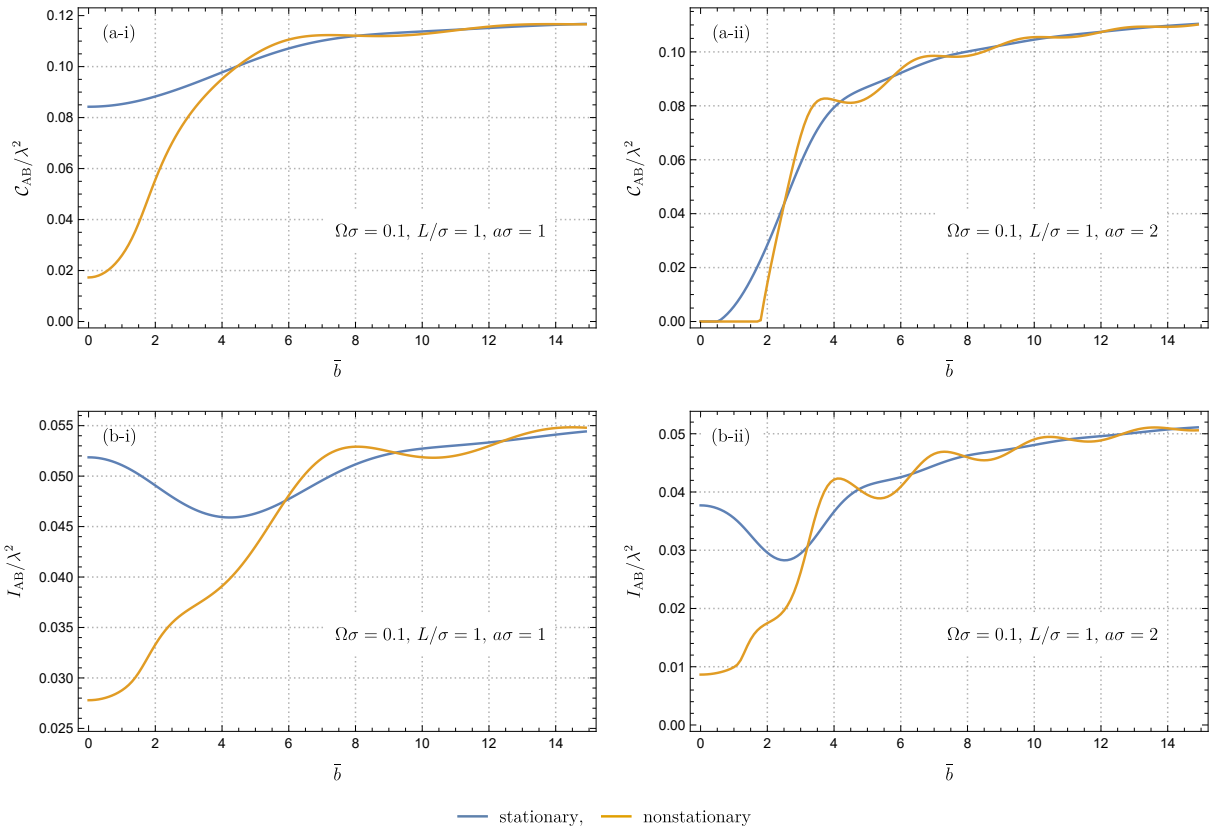

Figure 4.4: Concurrence (a) and quantum mutual information (b) harvested by stationary and nonstationary detectors as a function of $\bar{b}$. For each case, $\Omega\sigma = 0.1$ and $L/\sigma = 1$. (a-i) and (b-i) are respectively $\mathcal{C}_{\rm AB}/\lambda^2$ and $I_{\rm AB}/\lambda^2$ when $a\sigma = 1$, while (a-ii) and (b-ii) are respectively $\mathcal{C}_{\rm AB}/\lambda^2$ and $I_{\rm AB}/\lambda^2$ when $a\sigma = 2$.

4.2.2 Concurrence and quantum mutual information between uniformly accelerating detectors

We now move on to the correlation harvesting protocol using two uniformly accelerating detectors, exploring both stationary and nonstationary configurations as described in section 4.1.2.

We first examine the difference between the stationary and nonstationary configurations by plotting concurrence $\mathcal{C}_{\rm AB}/\lambda^2$ and quantum mutual information $I_{\rm AB}/\lambda^2$ as a function of $\bar{b}$ in figure 4.4. In these plots, we fix $\Omega\sigma = 0.1$ and $L/\sigma = 1$, and consider $a\sigma = 1$ and $a\sigma = 2$. We notice two characteristics: (i) In the vicinity of $\bar{b} \approx 0$, stationary detectors consistently harvest greater correlations than nonstationary detectors, for both concurrence and mutual information. (ii) As $\bar{b}$ becomes larger, both plots begin to oscillate with $\bar{b}$, and the curve representing correlations harvested by nonstationary detectors oscillates around the curve for the stationary case. The frequency of the oscillation increases as $a\sigma$ grows.

These observations can be traced back to the form of the Wightman functions (4.20) and (4.27). Let us recall that the denominators of these expressions contain $\sinh(x)$ when $\bar{b} \in [0, 1)$ and transform into $\sin(x)$ when $\bar{b} > 1$. Therefore, within the range $\bar{b} \in [0, 1)$, the correlations are characterized by an exponential pattern, while for $\bar{b} > 1$, an oscillatory behavior emerges. These traits explain the observation above. In particular, the suppression of correlations near $\bar{b} \approx 0$ for nonstationary detectors can be attributed to an additional term in the denominator of (4.27), which is absent in the stationary Wightman function (4.20). This extra term diminishes the amount of harvested correlations relative to the stationary scenario, and simultaneously gives rise to the oscillations noticed in the nonstationary case around the stationary one.

We next examine the acceleration dependence of concurrence $\mathcal{C}_{\rm AB}$ and quantum mutual information $I_{\rm AB}$ as illustrated in figures 4.5(a) and (b), respectively. The stationary (figure 4.5(a-i) and (b-i)) and nonstationary (figure 4.5(a-ii) and (b-ii)) configurations are depicted, and all four uniformly accelerated motions, linear ($\bar{b} = 0$), catenary ($\bar{b} = 0.5$), cusped ($\bar{b} = 1$), and circular ($\bar{b} = 2$) are shown in each figure.

As pointed out earlier, the correlations harvested by nonstationary detectors for $\bar{b} \in [0, 1)$ (figure 4.5(a-ii) and (b-ii)) decay with increasing $a\sigma$ faster than those extracted by the stationary detectors (figure 4.5(a-i) and (b-i)). Meanwhile, the correlations extracted by nonstationary detectors in circular motion ($\bar{b} > 1$) (figure 4.5(a-ii) and (b-ii)) exhibit oscillatory behavior around the corresponding stationary curves (figure 4.5(a-i) and (b-i)).

Another observation we make is that, for both stationary and nonstationary configurations and for any value of $\bar{b}$, $\mathcal{C}_{\rm AB}/\lambda^2$ becomes 0 at sufficiently high $a\sigma$. This can

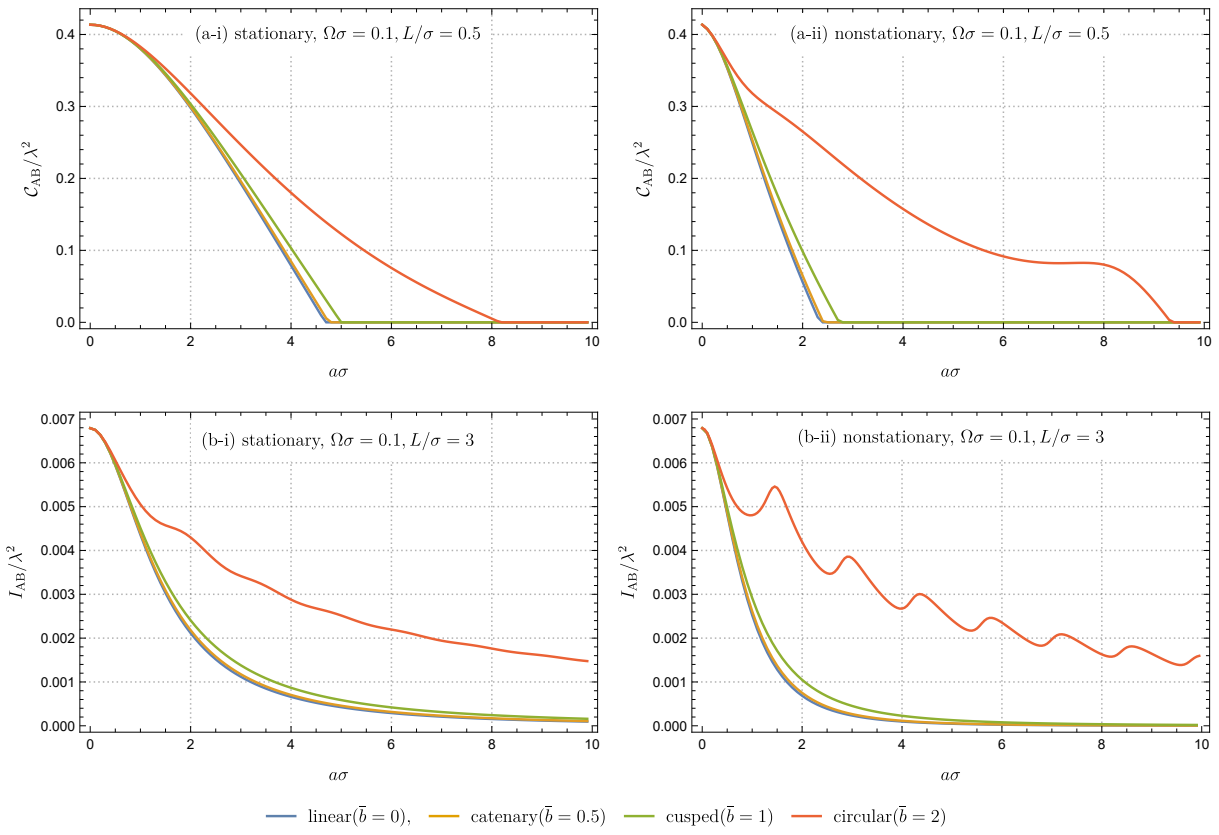

Figure 4.5: Concurrence $\mathcal{C}_{\rm AB}/\lambda^2$ with $\Omega\sigma = 0.1, L/\sigma = 0.5$ (a) and quantum mutual information $I_{\rm AB}/\lambda^2$ with $\Omega\sigma = 0.1, L/\sigma = 3$ (b) as a function of the magnitude of acceleration $a\sigma$. (a-i) and (b-i) correspond to the stationary configuration while (a-ii) and (b-ii) show the nonstationary one, and each figure has four curves indicating four different motions.

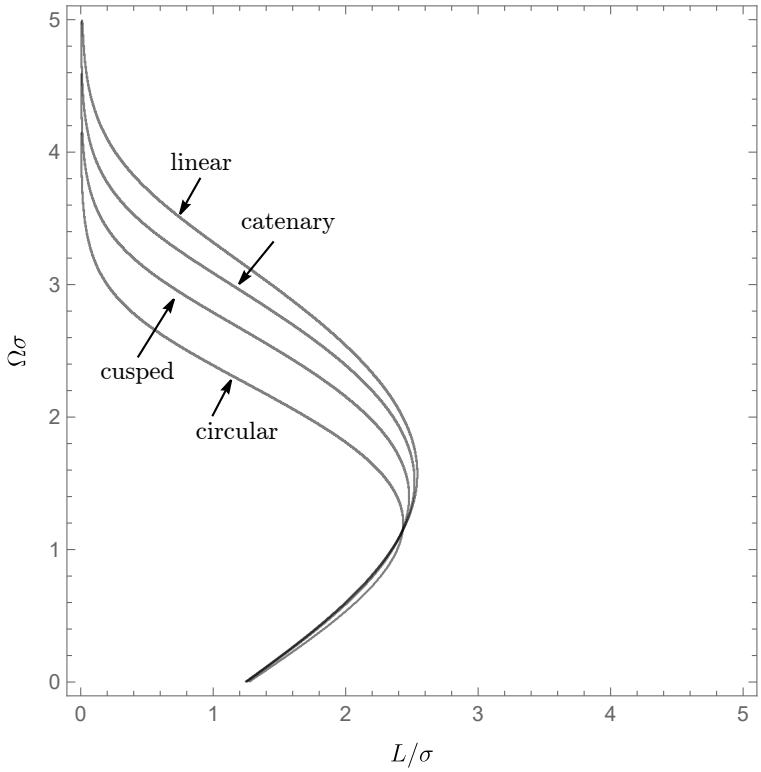

Figure 4.6: The boundaries between $\mathcal{C}_{\rm AB} > 0$ and $\mathcal{C}_{\rm AB} = 0$ for the four stationary trajectories as a function of the proper separation L/σ and the energy gap $\Omega\sigma$. Here, linear ($\bar{b} = 0$), catenary ($\bar{b} = 0.5$), cusped ($\bar{b} = 1$), and circular ($\bar{b} = 2$) with $a\sigma = 1$ are depicted. Concurrence is nonzero in the left region of each curve.

be attributed to the high transition probability at large $a\sigma$ as shown in figure 4.3(a), leading to $|\mathcal{M}| < \sqrt{\mathcal{L}_{\rm AA}\mathcal{L}_{\rm BB}}$ in (2.35). Furthermore, the high accelerations prevent the detectors from extracting quantum mutual information, as $I_{\rm AB}/\lambda^2 \to 0$ at $a\sigma \to \infty$ in figure 4.5(b). This indicates that any correlations cannot be harvested as $a\sigma \to \infty$ if the detectors are uniformly accelerated. These findings are consistent with previous results [56, 38, 57, 58, 55, 44, 59], where linearly and circularly accelerated detectors are considered. We extended these insights, providing a more general understanding that encompasses arbitrary uniformly accelerated motion.

4.2.3 Genuine Harvesting

We finally consider how much of the entanglement comes from the quantum field. We will call this type of entanglement genuine harvesting, which differs from entanglement in which the detectors are in causal contact (known as communication-assisted entanglement). As we mentioned in 2.1.2, the Wightman function can be decomposed into two parts: the anticommutator and the commutator of the field operator. The anticommutator part $\langle\{\hat{\phi}(\mathsf{x}),\hat{\phi}(\mathsf{x}')\}\rangle_{\rho_\phi}$ (the Hadamard function), where $\langle\cdot\rangle_{\rho_\phi}$ is the expectation value with respect to the field state ρ_ϕ, depends on the state of the field ρ_ϕ. Conversely, the commutator part $\langle[\hat{\phi}(\mathsf{x}),\hat{\phi}(\mathsf{x}')]\rangle_{\rho_\phi} = [\hat{\phi}(\mathsf{x}),\hat{\phi}(\mathsf{x}')] \in \mathbb{C}$ (the Pauli-Jordan function) is state-independent. This means that even if the field state is not entangled, the commutator part in the Wightman function allows detectors to be entangled with each other. Such entanglement does not come from preexisting entanglement in the field; rather it is associated with communication between the detectors, and thus we cannot say (for an unentangled field state) that entanglement is 'extracted' from the field if the commutator part is the only contribution [60]. We say that entanglement is harvested if the anticommutator contribution in the element $\mathcal{M}$ is nonzero, and in particular we qualify the harvested entanglement as being *genuine* if the commutator part in $\mathcal{M}$ is zero. Microcausality tells us that the two detectors can harvest genuine entanglement if they are causally disconnected. Here, we explore the circumstances under which two uniformly accelerating detectors can extract genuine entanglement from the field. Remarkably we find that this can be possible even if the detectors are in causal contact.

We begin by plotting the concurrence $\mathcal{C}_{\mathrm{AB}}/\lambda^2$ as a function of the proper separation L/σ between the detectors and the energy gap $\Omega\sigma$ in figure 4.6. The respective curves correspond to linear ($\bar{b} = 0$), catenary ($\bar{b} = 0.5$), cusped ($\bar{b} = 1$), and circular motions ($\bar{b} = 2$) in the stationary configurations depicted in figure 4.2. The left region of each curve represents the parameters $(L/\sigma, \Omega\sigma)$ that enable the detectors to become entangled, manifest as $\mathcal{C}_{\mathrm{AB}}/\lambda^2 > 0$. Conversely, the right region corresponds to $\mathcal{C}_{\mathrm{AB}}/\lambda^2 = 0$. Therefore, the stationary linear configuration ($\bar{b} = 0$) has the broadest parameter space that leads to $\mathcal{C}_{\mathrm{AB}}/\lambda^2 > 0$ compared to any other stationary configurations.

It has been shown [31] that two detectors at rest in Minkowski spacetime with a Gaussian switching function can be entangled with an arbitrary detector separation L/σ if the energy gap $\Omega\sigma$ is large enough. However, we see that this is not the case for uniformly accelerating detectors – they can be entangled only when they are close to each other, no matter how large $\Omega\sigma$ is.

We further ask how much entanglement stems from the anticommutator and commutator parts in the Wightman function. To see this, let us decompose the Wightman function

as

$$W(\mathsf{x},\mathsf{x}') = \mathrm{Re}[W(\mathsf{x},\mathsf{x}')] + \mathsf{i}\,\mathrm{Im}[W(\mathsf{x},\mathsf{x}')]\,, \tag{4.29}$$

where

$$2\mathrm{Re}[W(\mathsf{x},\mathsf{x}')] = \langle 0|\{\hat{\phi}(\mathsf{x}),\hat{\phi}(\mathsf{x}')\}|0\rangle\ , \tag{4.30a}$$

$$2\mathrm{Im}[W(\mathsf{x},\mathsf{x}')] = -\mathsf{i}\,[\hat{\phi}(\mathsf{x}),\hat{\phi}(\mathsf{x}')]\,. \tag{4.30b}$$

Then the matrix element $\mathcal{M}$ can be decomposed into

$$\mathcal{M} = \mathcal{M}_+ + \mathsf{i}\mathcal{M}_-\,, \tag{4.31}$$

where $\mathcal{M}_+$ and $\mathcal{M}_-$ are (2.32b) with the Wightman function being replaced by $\mathrm{Re}[W(\mathsf{x},\mathsf{x}')]$ and $\mathrm{Im}[W(\mathsf{x},\mathsf{x}')]$, respectively. $\mathcal{M}_+$ contains the information about the genuine entanglement whereas $\mathcal{M}_-$ is state-independent and does not necessarily exhibit the preexisted entanglement in the field. For the stationary detectors, these expressions can be simplified to single integral forms

$$\begin{aligned}\mathcal{M}_+ &= -\lambda^2\sigma\sqrt{\pi}e^{-\Omega^2\sigma^2}\int_0^\infty \mathrm{d}u\, e^{-u^2/4\sigma^2}W_{\mathrm{s}}(u) - \lambda^2\sigma\sqrt{\pi}e^{-\Omega^2\sigma^2}\int_0^\infty \mathrm{d}u\, e^{-u^2/4\sigma^2}W^*_{\mathrm{s}}(u)\\ &= -\lambda^2\sigma\sqrt{\pi}e^{-\Omega^2\sigma^2}\int_0^\infty \mathrm{d}u\, e^{-u^2/4\sigma^2}\left(W_{\mathrm{s}}(u)+W^*_{\mathrm{s}}(u)\right),\end{aligned} \tag{4.32a}$$

$$\begin{aligned}\mathcal{M}_- &= \mathsf{i}\lambda^2\sigma\sqrt{\pi}e^{-\Omega^2\sigma^2}\int_0^\infty \mathrm{d}u\, e^{-u^2/4\sigma^2}W_{\mathrm{s}}(u) - \mathsf{i}\lambda^2\sigma\sqrt{\pi}e^{-\Omega^2\sigma^2}\int_0^\infty \mathrm{d}u\, e^{-u^2/4\sigma^2}W^*_{\mathrm{s}}(u)\\ &= \mathsf{i}\lambda^2\sigma\sqrt{\pi}e^{-\Omega^2\sigma^2}\int_0^\infty \mathrm{d}u\, e^{-u^2/4\sigma^2}\left(W_{\mathrm{s}}(u)-W^*_{\mathrm{s}}(u)\right).\end{aligned} \tag{4.32b}$$

We then define harvested concurrence $\mathcal{C}^+_{\mathrm{AB}}$ and communication-assisted concurrence $\mathcal{C}^-_{\mathrm{AB}}$ as [60]

$$\mathcal{C}^\pm_{\mathrm{AB}} \coloneqq 2\max\{0,\ |\mathcal{M}_\pm| - \sqrt{\mathcal{L}_{\mathrm{AA}}\mathcal{L}_{\mathrm{BB}}}\} + \mathcal{O}(\lambda^4)\,. \tag{4.33}$$

We plot $\mathcal{C}^\pm_{\mathrm{AB}}/\lambda^2$ as a function of L/σ in figure 4.7. Here, we specifically choose the stationary linear ($\bar{b}=0$) and circular ($\bar{b}=2$) cases as a demonstration. We find that for $\Omega\sigma = 1$ (figure 4.7(a)), the detectors can harvest entanglement since $\mathcal{C}^+_{\mathrm{AB}}/\lambda^2 > 0$. Most strikingly, it is possible to extract genuine entanglement for $L/\sigma \in (1.5, 2.2)$ since $\mathcal{C}^+_{\mathrm{AB}} > 0$ while $\mathcal{C}^-_{\mathrm{AB}} = 0$ in this region. However, this is not always true as one can see

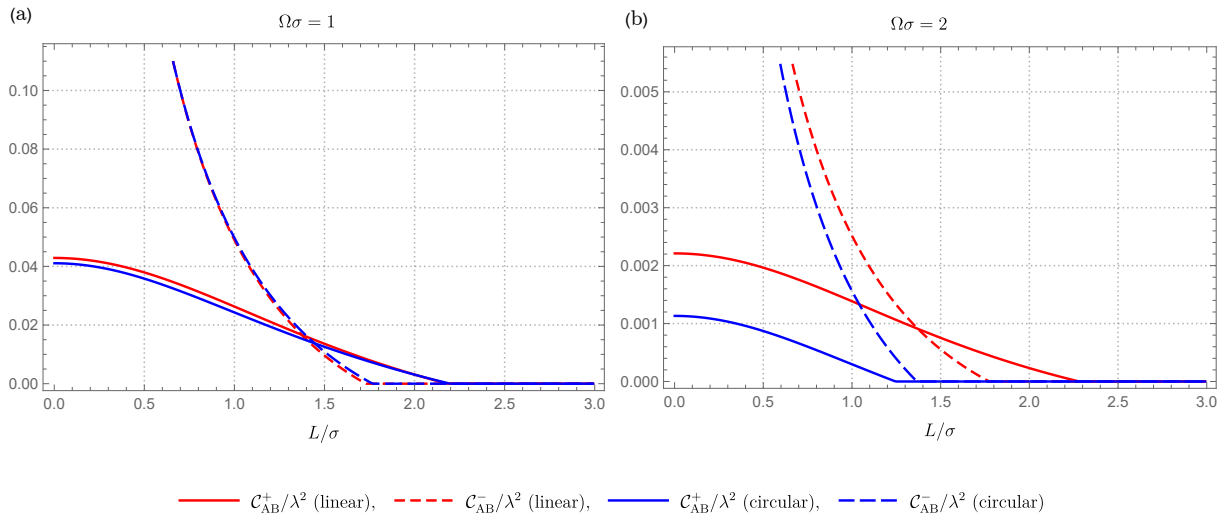

Figure 4.7: Harvested and communication-assisted concurrence $\mathcal{C}^{\pm}_{\mathrm{AB}}/\lambda^2$ for the stationary linear and circular configurations as a function of the detector separation L/σ. (a) When $\Omega\sigma = 1$. The linear and circular cases are very similar and the detectors can harvest genuine entanglement near $L/\sigma = 2$. (b) When $\Omega\sigma = 2$. Although the linear case does not change much compared to the $\Omega\sigma = 1$ case, the circular case cannot harvest genuine entanglement anymore. It is the mixture of the anticommutator and commutator contributions, or in the worst case $\mathcal{C}^{+}_{\mathrm{AB}}/\lambda^2 = 0$ around $L/\sigma = 1.3$.

from figure 4.7(b) when $\Omega\sigma = 2$. Here, detectors in circular motion can encounter the case where $\mathcal{C}^{+}_{\mathrm{AB}} = 0$ while $\mathcal{C}^{-}_{\mathrm{AB}} > 0$, which indicates that the generated entanglement after the interaction is purely coming from the communication and not from the field. However genuine entanglement can still be extracted in the linear configuration as shown in Fig 4.7(b).

4.3 Summary

We carried out the correlation harvesting protocol using two uniformly accelerating Unruh-DeWitt (UDW) detectors in (3+1)-dimensional Minkowski spacetime. According to Letaw [3], trajectories with constant (nonzero) acceleration can be characterized by the magnitude of the acceleration and two torsion parameters, resulting in five classes of motion: linear, catenary, cusped, circular, and helix. The first four of these classes of motion are confined

to a two-dimensional spatial surface and can be regarded as specific cases of the helix motion. Since two-dimensional configurations are more amenable to experimental setups, we employed these four simpler motions for our analysis.

We first examined the transition probability of a single detector following the four trajectories in section 4.2.1. Utilizing a unified expression for the Wightman functions along these trajectories, we were able to explore the general characteristics that are common to all these motions. We found that the transition probabilities of these motions monotonically increase with the magnitude of acceleration. Moreover, we also evaluated the effective temperature—an estimator for the temperature as observed by a detector.

We then introduced another UDW detector to consider the correlation harvesting protocol in Sec. 4.2.2. Two configurations were explored: stationary and nonstationary configurations. In the stationary configuration, detectors are separated in the direction perpendicular to their two-dimensional spatial planes of motion. Specifically, the displacement vector pointing from one detector to the other remains orthogonal to the velocity vectors of the detectors. In such a case, the Wightman function along the stationary configuration is time-translation invariant. On the other hand, in the nonstationary configuration, the displacement vector aligns parallel to the planes of motion. This makes the Wightman function nonstationary (i.e., not time-translation invariant). Moreover, while this Wightman function shares a common term with the stationary configuration, an additional term appears that specifically characterizes the nonstationary nature of this configuration.

We found that the harvested correlations—entanglement and total correlations—behave in a distinct manner depending on the motion of the detectors. Specifically, detectors in linear, catenary, and cusped motions within the nonstationary configuration gain fewer correlations compared to those in the stationary configuration. On the other hand, in the circular motion case, both configurations exhibit similar behavior. This difference can be attributed to the Wightman functions. For linear, catenary, and cusped motions, the Wightman function contain hyperbolic functions, leading to an exponential alteration of the results. In contrast, the Wightman function for circular motion is governed by trigonometric functions.

We also looked into the acceleration dependence of the harvested correlations and concluded (not surprisingly) that high accelerations prevent the detectors from acquiring correlations from the field. This point is consistent with previous papers [56, 38, 57, 58, 55, 44, 59], in which linearly and circularly accelerated detectors are considered. Our paper generalized these results to any uniformly accelerating detectors on two-dimensional spatial surfaces.

Finally, we focused on entanglement harvested by the detectors in the stationary con-

figuration and asked how much of entanglement is coming from the correlations preexisted in the field. To be precise, the entanglement coming from the commutator part of the Wightman function is state-independent, which suggests that the detectors can still be correlated even if the field is not entangled [60]. Thus, it is important to examine how the anticommutator part of the Wightman function (which is state-dependent) contributes to the extracted correlations. One way to eliminate the commutator contribution is to use causally disconnected detectors. However, we found that the existence of acceleration prohibits extraction of correlations with detectors separated far away, no matter what the energy gap is. However we also found the striking result that detectors in causal contact can genuinely harvest entanglement in certain parameter regimes.

Our results have important implications for experiment. Attempts to realize the Unruh effect and correlation harvesting generally rely on using laser pulses to probe what are effectively two dimensional surfaces. To probe the effects of non-inertial motion on mutual information and entanglement will therefore involve two detectors (two pulses) in nonstationary configurations, since only these can be realized in a two-dimensional setting. Experimental verification of the harvesting of genuine entanglement would be an exciting confirmation of our understanding of relativistic quantum information.

Chapter 5

Conclusion

We have studied the correlation harvesting protocol between two UDW detectors uniformly accelerating within the Minkowski vacuum. Our aim was to investigate the effects of uniform acceleration on the correlation harvesting protocol, with a particular emphasis on understanding the impact of Unruh temperature on total correlation harvesting. This effect was contrasted with other types of temperature dependencies, such as thermal bath temperature. Furthermore, in light of ongoing experiments aiming for Unruh effect verification, we were motivated to broaden our investigation to other uniformly accelerating trajectories that could induce similar effects to the Unruh effect, but might be more feasible in an experimental setting. Our main findings are:

- high accelerations(equivalently Unruh temperature) prevent the detectors from acquiring correlations from the field in all trajectories of detectors that are uniformly accelerating.
- Detectors in causal contact can genuinely harvest entanglement in certain parameter regimes.
- Unruh temperature affects the total correlation harvesting different than thermal bath temperature, despite their similar effect on a single detector.

We commenced in Chapter 3 by examining the harvesting protocol for mutual information using two uniformly accelerating detectors in linear motion. We considered three types of acceleration scenarios: parallel, anti-parallel, and perpendicular. Our findings revealed that acceleration can assist mutual information for specific detector separations

and energy gaps, while the mutual information asymptotically diminishes as acceleration (or equivalently, the Unruh temperature) increases. This illustrates that the effect of Unruh temperature on mutual information harvesting contrasts with two inertial detectors in a thermal bath [42, 43], where mutual information grows with the thermal bath's temperature. Additionally, we investigated the dependency on the energy gap and identified specific ranges of energy gaps where either classical correlations or nondistillable entanglement can be extracted from the field. The key insight from this study is that the temperature dependency of harvested correlations varies across different scenarios, even if a single detector exhibits consistent reactions in each case. This variability is anticipated, as the harvested correlation properties rely on the Wightman function. If the Wightman function exhibits differing functional forms given the field's state and the detectors' trajectories, diverse outcomes for correlation harvesting should be expected. Conversely, if the functional forms of Wightman functions are identical, the harvested correlations would manifest similar behavior.

In Chapter 4, we extended our investigations to consider a broader set of trajectories with constant (nonzero) acceleration, characterized by the magnitude of the acceleration and two torsion parameters. This resulted in five classes of uniform motion: linear, catenary, cusped, circular, and helix motions [3]. The first four classes, confined to a two-dimensional spatial surface, can be regarded as specific cases of helix motion. Since two-dimensional configurations are more amenable to experimental setups, we utilized these four simpler motions for our analysis. We examined the transition probability of a single detector following these trajectories and, utilizing a unified expression for the Wightman functions, explored the general characteristics common to all these motions.

Our findings indicated that the transition probabilities of these motions monotonically increase with the magnitude of acceleration. We subsequently studied the correlation harvesting protocol of two UDW detectors considering stationary and nonstationary configurations. Our results demonstrated that the harvested correlations—entanglement and total correlations—behave distinctly depending on the motion of the detectors. Specifically, detectors in linear, catenary, and cusped motions within the nonstationary configuration gain fewer correlations compared to those in the stationary configuration, while in the circular motion case, both configurations exhibit similar behavior. This difference is attributed to the nature of the Wightman functions; in the linear, catenary, and cusped motions, they contain hyperbolic functions, leading to exponential alteration of the results, while the Wightman function for circular motion is governed by trigonometric functions. We have also investigated the effect of acceleration on harvested correlations and concluded that high accelerations prevent the detectors from acquiring correlations from the field. This aligns with previous studies [56, 38, 57, 58, 55, 44, 59], with generalizing these re-

sults to uniformly accelerating detectors on two-dimensional spatial surfaces. Finally, we examined the presence of genuine entanglement (entanglement preexistent in the field) in the stationary configuration case, finding that the existence of acceleration prohibits the extraction of correlations with detectors separated far away, regardless of the energy gap. However, we also found the striking result that detectors in causal contact can harvest genuine entanglement in certain parameter regimes.

In view of the ongoing experiments aimed at verifying the Unruh temperature [81, 82, 83], our findings carry significant implications that could provide insights into more efficient methodologies for conducting such investigations. Potential directions for future research may include extending the study to investigating the correlation harvesting protocol of accelerating detectors in curved spacetime, incorporating additional detectors to examine the consequent alterations in the dynamics of the correlation harvesting protocol, and exploring the nuanced behavior of genuine entanglement under these expanded conditions.

References

[1] W. G. Unruh. Notes on black-hole evaporation. *Phys. Rev. D*, 14:870–892, Aug 1976. doi: 10.1103/PhysRevD.14.870. URL https://link.aps.org/doi/10.1103/PhysRevD.14.870. iv, 1, 2, 10

[2] Petar Simidzija and Eduardo Martín-Martínez. Harvesting correlations from thermal and squeezed coherent states. *Phys. Rev. D*, 98:085007, Oct 2018. doi: 10.1103/PhysRevD.98.085007. URL https://link.aps.org/doi/10.1103/PhysRevD.98.085007. iv

[3] John R. Letaw. Stationary world lines and the vacuum excitation of noninertial detectors. *Phys. Rev. D*, 23:1709–1714, Apr 1981. doi: 10.1103/PhysRevD.23.1709. URL https://link.aps.org/doi/10.1103/PhysRevD.23.1709. iv, 4, 27, 28, 45, 49

[4] A. Retzker, J. I. Cirac, M. B. Plenio, and B. Reznik. Methods for Detecting Acceleration Radiation in a Bose-Einstein Condensate. *Phys. Rev. Lett.*, 101:110402, Sep 2008. doi: 10.1103/PhysRevLett.101.110402. URL https://link.aps.org/doi/10.1103/PhysRevLett.101.110402. iv, 4

[5] Jamir Marino, Gabriel Menezes, and Iacopo Carusotto. Zero-point excitation of a circularly moving detector in an atomic condensate and phonon laser dynamical instabilities. *Phys. Rev. Res.*, 2:042009, Oct 2020. doi: 10.1103/PhysRevResearch.2.042009. URL https://link.aps.org/doi/10.1103/PhysRevResearch.2.042009. iv, 4

[6] Cisco Gooding, Steffen Biermann, Sebastian Erne, Jorma Louko, William G. Unruh, Jörg Schmiedmayer, and Silke Weinfurtner. Interferometric Unruh Detectors for Bose-Einstein Condensates. *Phys. Rev. Lett.*, 125:213603, Nov 2020. doi: 10.1103/PhysRevLett.125.213603. URL https://link.aps.org/doi/10.1103/PhysRevLett.125.213603. iv, 4

[7] Cameron R. D. Bunney and Jorma Louko. Circular motion analogue Unruh effect in a $2+1$ thermal bath: Robbing from the rich and giving to the poor. *Classical and Quantum Gravity*, 40(15):155001, 2023. doi: 10.1088/1361-6382/acde3b. URL https://iopscience.iop.org/article/10.1088/1361-6382/acde3b. iv, 4, 38

[8] Steffen Biermann, Sebastian Erne, Cisco Gooding, Jorma Louko, Jörg Schmiedmayer, William G. Unruh, and Silke Weinfurtner. Unruh and analogue Unruh temperatures for circular motion in $3+1$ and $2+1$ dimensions. *Phys. Rev. D*, 102:085006, Oct 2020. doi: 10.1103/PhysRevD.102.085006. URL https://link.aps.org/doi/10.1103/PhysRevD.102.085006. iv, 4, 38

[9] Cameron R. D. Bunney, Steffen Biermann, Vitor S. Barroso, August Geelmuyden, Cisco Gooding, Grégoire Ithier, Xavier Rojas, Jorma Louko, and Silke Weinfurtner. Third sound detectors in accelerated motion, 2023. iv, 4

[10] Steven Weinberg. *The Quantum Theory of Fields*, volume 1. Cambridge University Press, 1995. 1

[11] A. Zee. *Quantum Field Theory in a Nutshell*. Princeton University Press, 2 edition, 2010. 1, 6

[12] S. W. Hawking. Particle creation by black holes. *Commun. Math. Phys.*, 43(3):199–220, 1975. doi: https://link.springer.com/article/10.1007/BF01608497. URL https://link.springer.com/article/10.1007/BF01608497. 1

[13] Sasha Haco, Stephen W Hawking, Malcolm J Perry, and Andrew Strominger. Black hole entropy and soft hair. *J. High Energy Phys.*, 2018(12):98, 2018. doi: https://doi.org/10.1007/JHEP12(2018)098. 1

[14] B. S. DeWitt. Quantum gravity: The new synthesis. In S. W. Hawking and W. Israel, editors, *General Relativity: An Einstein Centenary Survey*, pages 680–745. Cambridge University Press, 1979. 1

[15] M. Cliche and A. Kempf. Relativistic quantum channel of communication through field quanta. *Phys. Rev. A*, 81:012330, Jan 2010. doi: 10.1103/PhysRevA.81.012330. URL https://link.aps.org/doi/10.1103/PhysRevA.81.012330. 1

[16] Robert H Jonsson. Quantum signaling in relativistic motion and across acceleration horizons. *Journal of Physics A: Mathematical and Theoretical*, 50(35):355401, 2017. doi: 10.1088/1751-8121/aa7d3c. 1

[17] André G. S. Landulfo. Nonperturbative approach to relativistic quantum communication channels. *Phys. Rev. D*, 93:104019, May 2016. doi: 10.1103/PhysRevD.93.104019. URL https://link.aps.org/doi/10.1103/PhysRevD.93.104019. 1

[18] Petar Simidzija, Aida Ahmadzadegan, Achim Kempf, and Eduardo Martín-Martínez. Transmission of quantum information through quantum fields. *Phys. Rev. D*, 101: 036014, Feb 2020. doi: 10.1103/PhysRevD.101.036014. URL https://link.aps.org/doi/10.1103/PhysRevD.101.036014. 1

[19] Erickson Tjoa and Kensuke Gallock-Yoshimura. Channel capacity of relativistic quantum communication with rapid interaction. *Phys. Rev. D*, 105:085011, Apr 2022. doi: 10.1103/PhysRevD.105.085011. URL https://link.aps.org/doi/10.1103/PhysRevD.105.085011. 1

[20] Paul M. Alsing and G. J. Milburn. Teleportation with a uniformly accelerated partner. *Phys. Rev. Lett.*, 91:180404, Oct 2003. doi: 10.1103/PhysRevLett.91.180404. URL https://link.aps.org/doi/10.1103/PhysRevLett.91.180404. 1

[21] André G. S. Landulfo and George E. A. Matsas. Sudden death of entanglement and teleportation fidelity loss via the Unruh effect. *Phys. Rev. A*, 80:032315, Sep 2009. doi: 10.1103/PhysRevA.80.032315. URL https://link.aps.org/doi/10.1103/PhysRevA.80.032315. 1

[22] Antony Valentini. Non-local correlations in quantum electrodynamics. *Phys. Lett.*, 153A(6):321 – 325, 1991. ISSN 0375-9601. doi: https://doi.org/10.1016/0375-9601(91)90952-5. URL http://www.sciencedirect.com/science/article/pii/0375960191909525. 1

[23] Benni Reznik. Entanglement from the vacuum. *Found. Phys.*, 33(1):167–176, 2003. doi: https://doi.org/10.1023/A:1022875910744. URL https://doi.org/10.1023/A:1022875910744. 1

[24] Benni Reznik, Alex Retzker, and Jonathan Silman. Violating Bell's inequalities in vacuum. *Phys. Rev. A*, 71:042104, Apr 2005. doi: 10.1103/PhysRevA.71.042104. URL https://link.aps.org/doi/10.1103/PhysRevA.71.042104. 1

[25] Stephen J. Summers and Reinhard Werner. The vacuum violates Bell's inequalities. *Phys. Lett.*, 110A(5):257 – 259, 1985. ISSN 0375-9601. doi: https://doi.org/10.1016/0375-9601(85)90093-3. URL http://www.sciencedirect.com/science/article/pii/0375960185900933. 2

[26] Stephen J. Summers and Reinhard Werner. Bell's inequalities and quantum field theory. i. general setting. *J. Math. Phys. (N.Y.)*, 28(10):2440–2447, 1987. doi: 10.1063/1.527733. URL https://doi.org/10.1063/1.527733. 2

[27] L Henderson and V Vedral. Classical, quantum and total correlations. *J. Phys. A*, 34(35):6899–6905, aug 2001. doi: 10.1088/0305-4470/34/35/315. URL https://iopscience.iop.org/article/10.1088/0305-4470/34/35/315. 2

[28] Harold Ollivier and Wojciech H. Zurek. Quantum discord: A measure of the quantumness of correlations. *Phys. Rev. Lett.*, 88:017901, Dec 2001. doi: 10.1103/PhysRevLett.88.017901. URL https://link.aps.org/doi/10.1103/PhysRevLett.88.017901. 2

[29] Eric G. Brown. Thermal amplification of field-correlation harvesting. *Phys. Rev. A*, 88:062336, Dec 2013. doi: 10.1103/PhysRevA.88.062336. URL https://link.aps.org/doi/10.1103/PhysRevA.88.062336. 2

[30] Abhisek Sahu, Irene Melgarejo-Lermas, and Eduardo Martín-Martínez. Sabotaging the harvesting of correlations from quantum fields. *Phys. Rev. D*, 105:065011, Mar 2022. doi: 10.1103/PhysRevD.105.065011. URL https://link.aps.org/doi/10.1103/PhysRevD.105.065011. 2

[31] Alejandro Pozas-Kerstjens and Eduardo Martín-Martínez. Harvesting correlations from the quantum vacuum. *Phys. Rev. D*, 92:064042, Sep 2015. doi: 10.1103/PhysRevD.92.064042. URL https://link.aps.org/doi/10.1103/PhysRevD.92.064042. 2, 5, 13, 14, 43

[32] Eduardo Martín-Martínez, Alexander R. H. Smith, and Daniel R. Terno. Spacetime structure and vacuum entanglement. *Phys. Rev. D*, 93:044001, Feb 2016. doi: 10.1103/PhysRevD.93.044001. URL https://link.aps.org/doi/10.1103/PhysRevD.93.044001. 2, 15

[33] S. Kukita and Y. Nambu. Harvesting large scale entanglement in de Sitter space with multiple detectors. *Entropy*, 19(9):449, Aug 2017. ISSN 1099-4300. doi: 10.3390/e19090449. URL http://dx.doi.org/10.3390/e19090449. 2

[34] Laura J Henderson, Robie A Hennigar, Robert B Mann, Alexander R H Smith, and Jialin Zhang. Harvesting entanglement from the black hole vacuum. *Classical Quantum Gravity*, 35(21):21LT02, oct 2018. URL https://doi.org/10.1088/1361-6382/aae27e. 2

[35] Keith K. Ng, Robert B. Mann, and Eduardo Martín-Martínez. Unruh-DeWitt detectors and entanglement: The anti–de Sitter space. *Phys. Rev. D*, 98:125005, Dec 2018. doi: 10.1103/PhysRevD.98.125005. URL https://link.aps.org/doi/10.1103/PhysRevD.98.125005. 2

[36] Wan Cong, Chen Qian, Michael R.R. Good, and Robert B. Mann. Effects of horizons on entanglement harvesting. *J. High Energy Phys.*, 10(2020):67, Oct 2020. ISSN 1029-8479. doi: 10.1007/JHEP10(2020)067. URL https://doi.org/10.1007/JHEP10(2020)067. 2

[37] Finnian Gray, David Kubizňák, Taillte May, Sydney Timmerman, and Erickson Tjoa. Quantum imprints of gravitational shockwaves. *J. High Energy Phys.*, 11(2021):054, 2021. doi: https://doi.org/10.1007/JHEP11(2021)054. 2

[38] Grant Salton, Robert B Mann, and Nicolas C Menicucci. Acceleration-assisted entanglement harvesting and rangefinding. *New J. Phys.*, 17(3):035001, mar 2015. doi: 10.1088/1367-2630/17/3/035001. 2, 5, 42, 46, 49

[39] Joshua Foo, Sho Onoe, and Magdalena Zych. Unruh-dewitt detectors in quantum superpositions of trajectories. *Phys. Rev. D*, 102:085013, Oct 2020. doi: 10.1103/PhysRevD.102.085013. URL https://link.aps.org/doi/10.1103/PhysRevD.102.085013. 2

[40] C. Suryaatmadja, R. B. Mann, and W. Cong. Entanglement harvesting of inertially moving unruh-dewitt detectors in minkowski spacetime. *Phys. Rev. D*, 106:076002, Oct 2022. doi: 10.1103/PhysRevD.106.076002. URL https://link.aps.org/doi/10.1103/PhysRevD.106.076002. 2

[41] Greg Ver Steeg and Nicolas C. Menicucci. Entangling power of an expanding universe. *Phys. Rev. D*, 79:044027, Feb 2009. doi: 10.1103/PhysRevD.79.044027. URL https://link.aps.org/doi/10.1103/PhysRevD.79.044027. 2, 24

[42] Eric G. Brown, Eduardo Martín-Martínez, Nicolas C. Menicucci, and Robert B. Mann. Detectors for probing relativistic quantum physics beyond perturbation theory. *Phys. Rev. D*, 87:084062, Apr 2013. doi: 10.1103/PhysRevD.87.084062. URL https://link.aps.org/doi/10.1103/PhysRevD.87.084062. 2, 22, 25, 49

[43] Petar Simidzija and Eduardo Martín-Martínez. Harvesting correlations from thermal and squeezed coherent states. *Phys. Rev. D*, 98:085007, Oct 2018. doi: 10.1103/PhysRevD.98.085007. URL https://link.aps.org/doi/10.1103/PhysRevD.98.085007. 2, 21, 22, 23, 24, 25, 26, 49

[44] Zhihong Liu, Jialin Zhang, and Hongwei Yu. Entanglement harvesting of accelerated detectors versus static ones in a thermal bath. *Phys. Rev. D*, 107:045010, Feb 2023. doi: 10.1103/PhysRevD.107.045010. URL https://link.aps.org/doi/10.1103/PhysRevD.107.045010. 2, 5, 42, 46, 49

[45] Matthew P. G. Robbins, Laura J. Henderson, and Robert B. Mann. Entanglement amplification from rotating black holes. *Classical Quantum Gravity*, 39(2):02LT01, 2022. URL https://doi.org/10.1088/1361-6382/ac08a8. 2

[46] Laura J. Henderson, Robie A. Hennigar, Robert B. Mann, Alexander R.H. Smith, and Jialin Zhang. Anti-hawking phenomena. *Physics Letters B*, 809:135732, 2020. ISSN 0370-2693. doi: https://doi.org/10.1016/j.physletb.2020.135732. URL https://www.sciencedirect.com/science/article/pii/S0370269320305359. 2

[47] Matthew P. G. Robbins and Robert B. Mann. Anti-hawking phenomena around a rotating btz black hole. *Phys. Rev. D*, 106:045018, Aug 2022. doi: 10.1103/PhysRevD.106.045018. URL https://link.aps.org/doi/10.1103/PhysRevD.106.045018. 2

[48] Laura J. Henderson, Su Yu Ding, and Robert B. Mann. Entanglement harvesting with a twist. *AVS Quantum Sci.*, 4(1):014402, 2022. doi: 10.1116/5.0078314. 2

[49] Lissa De Souza Campos and Claudio Dappiaggi. The anti-Hawking effect on a BTZ black hole with Robin boundary conditions. *Phys. Lett. B*, 816:136198, 2021. doi: 10.1016/j.physletb.2021.136198. 2

[50] Erickson Tjoa and Robert B Mann. Harvesting correlations in Schwarzschild and collapsing shell spacetimes. *J. High Energy Phys.*, 08(2020):155, 2020. doi: https://doi.org/10.1007/JHEP08(2020)155. 2

[51] Kensuke Gallock-Yoshimura, Erickson Tjoa, and Robert B. Mann. Harvesting entanglement with detectors freely falling into a black hole. *Phys. Rev. D*, 104:025001, Jul 2021. doi: 10.1103/PhysRevD.104.025001. URL https://link.aps.org/doi/10.1103/PhysRevD.104.025001. 2

[52] C.H. Bennett, P.W. Shor, J.A. Smolin, and A.V. Thapliyal. Entanglement-assisted capacity of a quantum channel and the reverse shannon theorem. *IEEE Transactions on Information Theory*, 48(10):2637–2655, 2002. doi: 10.1109/TIT.2002.802612. 3

[53] Tomohiro Ogawa. Perfect quantum error-correcting condition revisited, 2005. URL https://arxiv.org/abs/quant-ph/0505167. 3

[54] Kendra Bueley, Luosi Huang, Kensuke Gallock-Yoshimura, and Robert B. Mann. Harvesting mutual information from btz black hole spacetime. *Phys. Rev. D*, 106: 025010, Jul 2022. doi: 10.1103/PhysRevD.106.025010. URL https://link.aps.org/doi/10.1103/PhysRevD.106.025010. 3

[55] Zhihong Liu, Jialin Zhang, Robert B. Mann, and Hongwei Yu. Does acceleration assist entanglement harvesting? *Phys. Rev. D*, 105(8):085012, 2022. doi: 10.1103/PhysRevD.105.085012. 3, 5, 16, 18, 21, 23, 24, 25, 35, 42, 46, 49

[56] Jason Doukas and Benedict Carson. Entanglement of two qubits in a relativistic orbit. *Phys. Rev. A*, 81:062320, Jun 2010. doi: 10.1103/PhysRevA.81.062320. URL https://link.aps.org/doi/10.1103/PhysRevA.81.062320. 5, 42, 46, 49

[57] Jialin Zhang and Hongwei Yu. Entanglement harvesting for unruh-dewitt detectors in circular motion. *Phys. Rev. D*, 102:065013, Sep 2020. doi: 10.1103/PhysRevD.102.065013. URL https://link.aps.org/doi/10.1103/PhysRevD.102.065013. 5, 42, 46, 49

[58] Zhihong Liu, Jialin Zhang, and Hongwei Yu. Entanglement harvesting in the presence of a reflecting boundary. *J. High Energy Phys.*, 08(2021):020, 2021. doi: https://doi.org/10.1007/JHEP08(2021)020. 5, 42, 46, 49

[59] Manar Naeem, Kensuke Gallock-Yoshimura, and Robert B. Mann. Mutual information harvested by uniformly accelerated particle detectors. *Phys. Rev. D*, 107:065016, Mar 2023. doi: 10.1103/PhysRevD.107.065016. URL https://link.aps.org/doi/10.1103/PhysRevD.107.065016. 5, 35, 42, 46, 49

[60] Erickson Tjoa and Eduardo Martín-Martínez. When entanglement harvesting is not really harvesting. *Phys. Rev. D*, 104:125005, Dec 2021. doi: 10.1103/PhysRevD.104.125005. URL https://link.aps.org/doi/10.1103/PhysRevD.104.125005. 5, 43, 44, 47

[61] N.D. Birrell and P.C.W. Davies. *Quantum Fields in Curved Space*. Cambridge Monographs on Mathematical Physics. Cambridge University Press, Cambridge, England, 1984. ISBN 9780521278584. URL https://books.google.ca/books?id=SEnaUnrqzrUC. 6, 24

[62] Ryogo Kubo. Statistical-mechanical theory of irreversible processes. i. general theory and simple applications to magnetic and conduction problems. *Journal of the Physical Society of Japan*, 12(6):570–586, 1957. doi: 10.1143/JPSJ.12.570. URL https://doi.org/10.1143/JPSJ.12.570. 9, 38, 61

[63] Paul C. Martin and Julian Schwinger. Theory of many-particle systems. i. *Phys. Rev.*, 115:1342–1373, Sep 1959. doi: 10.1103/PhysRev.115.1342. URL https://link.aps.org/doi/10.1103/PhysRev.115.1342. 9, 38, 61

[64] Eduardo Martín-Martínez and Pablo Rodriguez-Lopez. Relativistic quantum optics: The relativistic invariance of the light-matter interaction models. *Phys. Rev. D*, 97: 105026, May 2018. doi: 10.1103/PhysRevD.97.105026. URL https://link.aps.org/doi/10.1103/PhysRevD.97.105026. 12

[65] Eduardo Martín-Martínez, T. Rick Perche, and Bruno de S. L. Torres. General relativistic quantum optics: Finite-size particle detector models in curved spacetimes. *Phys. Rev. D*, 101:045017, Feb 2020. doi: 10.1103/PhysRevD.101.045017. URL https://link.aps.org/doi/10.1103/PhysRevD.101.045017. 12

[66] Pratyusha Chowdhury and Bibhas Ranjan Majhi. Fate of entanglement between two Unruh-DeWitt detectors due to their motion and background temperature. *JHEP*, 05:025, 2022. doi: 10.1007/JHEP05(2022)025. 13

[67] Dyuman Bhattacharya, Kensuke Gallock-Yoshimura, Laura J. Henderson, and Robert B. Mann. Extraction of entanglement from quantum fields with entangled particle detectors, 12 2022. 13

[68] Sam A. Hill and William K. Wootters. Entanglement of a Pair of Quantum Bits. *Phys. Rev. Lett.*, 78:5022–5025, Jun 1997. doi: 10.1103/PhysRevLett.78.5022. URL https://link.aps.org/doi/10.1103/PhysRevLett.78.5022. 14

[69] William K. Wootters. Entanglement of formation of an arbitrary state of two qubits. *Phys. Rev. Lett.*, 80:2245–2248, Mar 1998. doi: 10.1103/PhysRevLett.80.2245. URL https://link.aps.org/doi/10.1103/PhysRevLett.80.2245. 14

[70] M.A. Nielsen and I.L. Chuang. *Quantum Computation and Quantum Information*. Cambridge Series on Information and the Natural Sciences. Cambridge University Press, Cambridge, England, 2000. ISBN 9780521635035. URL https://books.google.ca/books?id=65FqEKQOfP8C. 14

[71] Yasusada Nambu and Yuji Ohsumi. Classical and quantum correlations of scalar field in the inflationary universe. *Phys. Rev. D*, 84:044028, Aug 2011. doi: 10.1103/PhysRevD.84.044028. URL https://link.aps.org/doi/10.1103/PhysRevD.84.044028. 24

[72] G. W. Gibbons and S. W. Hawking. Cosmological event horizons, thermodynamics, and particle creation. *Phys. Rev. D*, 15:2738–2751, May 1977. doi: 10.1103/PhysRevD.15.2738. URL https://link.aps.org/doi/10.1103/PhysRevD.15.2738. 24

[73] Michael Good, Benito A. Juárez-Aubry, Dimitris Moustos, and Maksat Temirkhan. Unruh-like effects: effective temperatures along stationary worldlines. *J. High Energy Phys.*, 06(2020):059, 2020. doi: https://doi.org/10.1007/JHEP06(2020)059. 30, 38

[74] W.G. Brenna, Robert B. Mann, and Eduardo Martín-Martínez. Anti-Unruh phenomena. *Physics Letters B*, 757:307 – 311, 2016. ISSN 0370-2693. doi: https://doi.org/10.1016/j.physletb.2016.04.002. URL http://www.sciencedirect.com/science/article/pii/S0370269316300727. 37

[75] Luis J. Garay, Eduardo Martín-Martínez, and José de Ramón. Thermalization of particle detectors: The Unruh effect and its reverse. *Phys. Rev. D*, 94:104048, Nov 2016. doi: 10.1103/PhysRevD.94.104048. URL https://link.aps.org/doi/10.1103/PhysRevD.94.104048. 37, 38

[76] Christopher J. Fewster, Benito A. Juárez-Aubry, and Jorma Louko. Waiting for Unruh. *Class. Quantum Grav.*, 33:165003, 2016. doi: https://doi.org/10.1088/0264-9381/33/16/165003. URL https://doi.org/10.1088/0264-9381/33/16/165003. 38, 62

[77] J.S. Bell and J.M. Leinaas. Electrons as accelerated thermometers. *Nuclear Physics B*, 212(1):131–150, 1983. ISSN 0550-3213. doi: https://doi.org/10.1016/0550-3213(83)90601-6. URL https://www.sciencedirect.com/science/article/pii/0550321383906016. 38

[78] J.S. Bell and J.M. Leinaas. The Unruh effect and quantum fluctuations of electrons in storage rings. *Nuclear Physics B*, 284:488–508, 1987. ISSN 0550-3213. doi: https://doi.org/10.1016/0550-3213(87)90047-2. URL https://www.sciencedirect.com/science/article/pii/0550321387900472. 38

[79] W.G. Unruh. Acceleration radiation for orbiting electrons. *Physics Reports*, 307(1):163–171, 1998. ISSN 0370-1573. doi: https://doi.org/10.1016/S0370-1573(98)00068-4. URL https://www.sciencedirect.com/science/article/pii/S0370157398000684. 38

[80] Benito A. Juárez-Aubry and Dimitris Moustos. Asymptotic states for stationary Unruh-DeWitt detectors. *Phys. Rev. D*, 100:025018, Jul 2019. doi: 10.1103/

PhysRevD.100.025018. URL https://link.aps.org/doi/10.1103/PhysRevD.100.025018. 38

[81] Ileana-Cristina Benea-Chelmus, Francesca Fabiana Settembrini, Giacomo Scalari, and Jérôme Faist. Electric field correlation measurements on the electromagnetic vacuum state. *Nature*, 568:202–206, 2019. doi: 10.1038/s41586-019-1083-9. URL https://doi.org/10.1038/s41586-019-1083-9. 50

[82] Francesca Fabiana Settembrini, Frieder Lindel, Alexa Marina Herter, Stefan Yoshi Buhmann, and Jérôme Faist. Detection of quantum-vacuum field correlations outside the light cone. *Nature Communications*, 13:3383, 2022. doi: 10.1038/s41467-022-31081-1. URL https://doi.org/10.1038/s41467-022-31081-1. 50

[83] Frieder Lindel, Alexa Herter, Jérôme Faist, and Stefan Yoshi Buhmann. How to Separately Probe Vacuum Field Fluctuations and Source Radiation in Space and Time. *arXiv:2305.06387*, 2023. URL https://arxiv.org/abs/2305.06387. 50

APPENDICES

.1 Effective temperature

Here, we review the concept of effective temperature T_{eff} and clarify its relation to the KMS temperature.

Let us first review the KMS temperature. In quantum theory with separable Hilbert spaces, a trace of an operator, $\mathrm{Tr}[\cdot]$ is well defined. This enables us to consider the Gibbs state at the inverse temperature β, $\rho = e^{-\beta\hat{H}}/Z$, where $Z \coloneqq \mathrm{Tr}[e^{-\beta\hat{H}}]$ is the partition function. This is what we consider a thermal state of a system.

However in QFT, a trace is generally not well defined. Instead, we identify the Kubo-Martin-Schwinger (KMS) state [62, 63] as a thermal state in QFT. Specifically, if the field is in the KMS thermal state with respect to time τ at the inverse KMS temperature β_{KMS}, the Wightman function satisfies

$$W(\Delta\tau - \mathsf{i}\beta_{\text{KMS}}) = W(-\Delta\tau)\,, \tag{1}$$

where $\Delta\tau \coloneqq \tau - \tau'$. The Fourier transform of this equality with respect to $\Delta\tau$ reads

$$\tilde{W}(-\omega) = e^{\beta_{\text{KMS}}\omega}\tilde{W}(\omega)\,. \tag{2}$$

This equality in the Fourier domain is known as the detailed balance condition. Thus, the thermality of a quantum field is imprinted in these equalities.

The thermality can also be implemented in the transition probability of a UDW detector. Recall that the transition probability is written as

$$\mathcal{L} = \lambda^2 \int_{\mathbb{R}} \mathrm{d}\tau \int_{\mathbb{R}} \mathrm{d}\tau'\, \chi(\tau)\chi(\tau') e^{-\mathsf{i}\Omega(\tau-\tau')} W\Big(\mathsf{x}(\tau), \mathsf{x}(\tau')\Big)\,, \tag{3}$$

where the subscript in $\mathcal{L}_{jj}$, $j \in \{\mathrm{A}, \mathrm{B}\}$ is omitted for simplicity. Let us assume that the switching function, $\chi(\tau)$, has a characteristic time length σ. In our paper, this is the

Gaussian width in $\chi(\tau) = e^{-\tau^2/2\sigma^2}$. It is convenient to introduce a quantity related to the transition probability known as the *response function* (divided by the characteristic time length) $\mathcal{F}(\Omega, \sigma)$:

$$\begin{aligned}
&\mathcal{L} = \lambda^2 \sigma \mathcal{F}(\Omega, \sigma)\,, \\
&\mathcal{F}(\Omega, \sigma) \coloneqq \\
&\quad \frac{1}{\sigma} \int_{\mathbb{R}} \mathrm{d}\tau \int_{\mathbb{R}} \mathrm{d}\tau'\, \chi(\tau)\chi(\tau') e^{-\mathrm{i}\Omega(\tau-\tau')} W\Big(\mathsf{x}(\tau), \mathsf{x}(\tau')\Big)\,.
\end{aligned} \tag{4}$$

If the field is in the KMS state and the switching function is a rapidly decreasing function such as a Gaussian function, then the response function in the long interaction limit obeys the detailed balance relation [76]:

$$\lim_{\sigma\to\infty} \frac{\mathcal{F}(-\Omega, \sigma)}{\mathcal{F}(\Omega, \sigma)} = e^{\beta_{\mathrm{KMS}}\Omega}\,. \tag{5}$$

Note that this relation holds when the long interaction limit is taken. On the other hand, if σ is not sufficiently long, the ratio of the response function (sometimes known as the excited-to-deexcited ratio) does not satisfy the detailed balance condition.

From this relation, one can define the *effective temperature* as

$$T_{\mathrm{eff}}^{-1} \coloneqq \frac{1}{\Omega} \ln \frac{\mathcal{F}(-\Omega, \sigma)}{\mathcal{F}(\Omega, \sigma)}\,. \tag{6}$$

Note that the effective temperature is not necessarily the KMS temperature. If the field is in the KMS state and the long interaction limit is taken, then the effective temperature becomes the KMS temperature. In this sense, the effective temperature is an estimator for the field's temperature.